Cell

Chaperonin-Catalyzed Rescue of Kinetically Trapped States in Protein Folding

Kausik Chakraborty,[1,4,5] Manal Chatila,[1,4] Jyoti Sinha,[1,4] Qiaoyun Shi,[1] Bernhard C. Poschner,[1] Martin Sikor,[2] Guoxin Jiang,[1] Don C. Lamb,[2,3] F. Ulrich Hartl,[1,*] and Manajit Hayer-Hartl[1,*]

[1]Department of Cellular Biochemistry, Max Planck Institute of Biochemistry (MPIB), Am Klopferspitz 18, 82152 Martinsried, Germany
[2]Physical Chemistry, Department of Chemistry, Center for Nanoscience, and Munich Center for Integrated Protein Science (CiPSM), Ludwig-Maximilians-Universität München, Butenandtstrasse 11, Gerhard-Ertl-Building, D-81377 Munich, Germany
[3]Department of Physics, University of Illinois at Urbana-Champaign, 1110 W. Green Street, Urbana, IL 61801, USA
[4]These authors contributed equally to this work
[5]Present address: Institute of Genomics and Integrative Biology (CSIR), Mall Road, Delhi 110007, India
*Correspondence: uhartl@biochem.mpg.de (F.U.H.), mhartl@biochem.mpg.de (M.H.-H.)
DOI 10.1016/j.cell.2010.05.027

SUMMARY

GroEL and GroES form a chaperonin nano-cage for single protein molecules to fold in isolation. The folding properties that render a protein chaperonin dependent are not yet understood. Here, we address this question using a double mutant of the maltose-binding protein DM-MBP as a substrate. Upon spontaneous refolding, DM-MBP populates a kinetically trapped intermediate that is collapsed but structurally disordered. Introducing two long-range disulfide bonds into DM-MBP reduces the entropic folding barrier of this intermediate and strongly accelerates native state formation. Strikingly, steric confinement of the protein in the chaperonin cage mimics the kinetic effect of constraining disulfides on folding, in a manner mediated by negative charge clusters in the cage wall. These findings suggest that chaperonin dependence correlates with the tendency of proteins to populate entropically stabilized folding intermediates. The capacity to rescue proteins from such folding traps may explain the uniquely essential role of chaperonin cages within the cellular chaperone network.

INTRODUCTION

Bacterial cells generally contain multiple, partly redundant chaperone systems that function in preventing the aggregation of newly synthesized and stress-denatured proteins (Frydman, 2001; Hartl and Hayer-Hartl, 2002). In contrast to all other components of this chaperone network, the chaperonin, GroEL, and its cofactor, GroES, are uniquely essential, forming a specialized nano-compartment for single protein molecules to fold in isolation (Brinker et al., 2001; Mayhew et al., 1996; Weissman et al., 1996). In view of the fact that only a limited number of proteins are GroEL/ES dependent, it has been suggested that the chaperonin, in addition to preventing aggregation, may actively rescue proteins from kinetic folding traps, thereby accelerating their folding speed (Hartl and Hayer-Hartl, 2009; Jewett and Shea, 2010). Elucidating the properties of the trapped folding intermediate from which the chaperonin catalyzes escape is essential for understanding the mechanism underlying this active process.

The structure and reaction cycle of the GroEL/ES system have been investigated extensively (Hartl and Hayer-Hartl, 2009; Horwich et al., 2009). GroEL is a cylindrical complex consisting of two heptameric rings of ~57 kDa subunits that are stacked back-to-back. Each subunit of GroEL is composed of an equatorial ATPase domain, an apical domain, and an intermediate hinge domain. The apical domains form the flexible ring opening and expose hydrophobic amino acid residues toward the central cavity for the binding of non-native substrate proteins (Figure 1A). GroES is a heptameric ring of ~10 kDa subunits that caps the substrate-bound ring of GroEL. This step is dependent on ATP binding to GroEL and results in the displacement of the substrate into an enclosed cage, large enough to accommodate proteins up to ~60 kDa. Upon binding of ATP and GroES, GroEL undergoes a dramatic conformational change that generates an enlarged hydrophilic cavity with a net-negative charge. The enclosed protein is free to fold for ~10 s, the time needed for ATP hydrolysis (Figure 1A). Subsequent ATP binding to the opposite GroEL ring causes the dissociation of GroES and the release of substrate. Non-native protein is rapidly recaptured by GroEL for another folding attempt.

GroEL-dependent proteins typically have complex domain topologies and are thought to populate kinetically trapped folding intermediates (Kerner et al., 2005). Passive prevention of aggregation by encapsulation in the GroEL/ES cage is required for their efficient folding. However, an active mechanism in promoting folding appears to operate in addition, based on the demonstration that GroEL/ES can substantially enhance the rate of folding for proteins such as bacterial Rubisco (~50 kDa) (Brinker et al., 2001). More recently, an ~10-fold

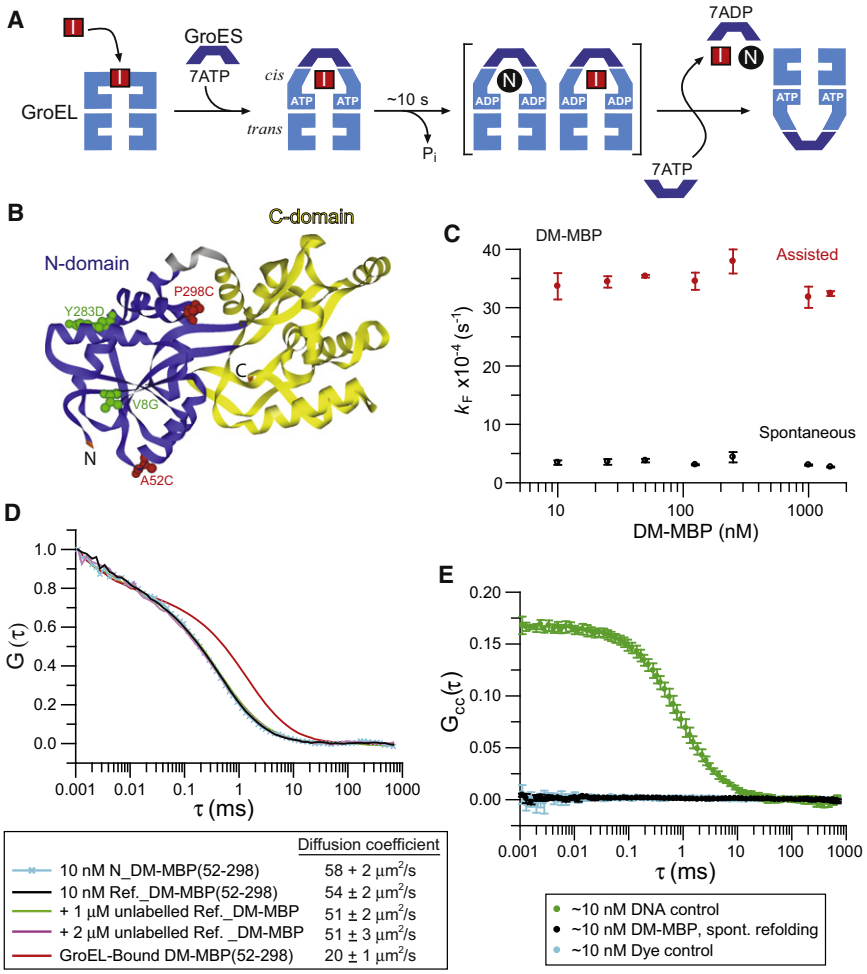

Figure 1. Rate of Spontaneous Refolding of DM-MBP Is Independent of Aggregation

(A) Schematic representation of refolding experiment with GroEL/ES. I, folding intermediate bound by the apical domains of GroEL; N, native protein. Note that substrates may undergo multiple rounds of GroEL binding and release; both I and N exit the cage after ~10 s upon ADP/GroES dissociation. I is then rapidly rebound by GroEL.

(B) Ribbon diagram of the structure of MBP (Spurlino et al., 1991; Protein Data Bank [PDB] 1OMP; DS Viewer-Pro), indicating the positions of DM-MBP mutations V8G and Y283D (green) and the cysteine mutations A52C and P298C (red) used for fluorescent labeling. The two discontinuous domains are shown in blue (N-domain) and yellow (C-domain).

(C) Rates of spontaneous and GroEL/ES-mediated refolding of DM-MBP at different DM-MBP concentrations (10 nM–1.5 μM). DM-MBP was denatured in 6 M GuHCl and diluted 100-fold to 60 mM GuHCl into buffer A (spontaneous) or buffer containing 0.5–4 μM GroEL and 1–8 μM GroES (assisted) at 25°C. Assisted refolding was initiated by the addition of 5 mM ATP. Refolding was monitored by Trp fluorescence. Standard deviations from three independent measurements.

(D) Fluorescence correlation spectroscopy (FCS) to measure the diffusion rates of spontaneously refolding DM-MBP. Normalized fluorescence autocorrelation amplitudes G(τ) are shown. Diffusion times were measured at 20°C during the first 800 s of refolding with 10 nM Atto532-labeled DM-MBP(52–298) in the absence or presence of 1 or 2 μM unlabeled, refolding DM-MBP(52–298) (final GuHCl 30 mM in buffer A). Native and GroEL-bound labeled DM-MBP(52–298) were used as controls (see Extended Experimental Procedures for details). Diffusion coefficients are given as averages ± standard deviation (SD) from three independent experiments.

(E) Fluorescence cross-correlation spectroscopy (FCCS) of a 1:1 mixture of DM-MBP(52–298) labeled at position 52 with Atto532 or Atto647N. Labeled DM-MBP molecules were denatured and diluted as in (D) to a final concentration of ~5 nM each. FCCS was recorded with pulsed interleaved excitation (PIE) (Muller et al., 2005) within 120 s of initiating refolding. Approximately 10 nM of DNA (40 base pair) labeled with Atto532 and Atto647 spaced 22 base pairs apart was used as a positive control and the same fluorophores freely diffusing in solution served as a negative control.

See also Figure S1 and Figure S2.

acceleration of folding was reported for a double mutant of the ~41 kDa maltose-binding protein (DM-MBP) (Tang et al., 2006). Different mechanisms have been proposed to explain how GroEL may catalyze the escape of these proteins from folding traps. One model suggests that steric confinement in the GroEL/ES cage destabilizes trapped intermediates (Brinker et al., 2001; Tang et al., 2006). According to another model, "forced" protein unfolding in consecutive rounds of chaperonin binding (iterative annealing) promotes the reversal of kinetically trapped states (Lin et al., 2008; Shtilerman et al., 1999). Consistent with such a mechanism, proteins undergo a conformational expansion on initial binding to GroEL and upon subsequent ATP-dependent movements of the apical GroEL domains (Lin et al., 2008; Sharma et al., 2008). However, accelerated folding also occurs during a single round of encapsulation in the chaperonin cage without such unfolding cycles (Brinker et al., 2001; Sharma et al., 2008; Tang et al., 2006, 2008), indicating that the physical environment of the cage is critical. Whereas both of these models argue for an active role of the chaperonin in promoting folding, a third model suggests that passive encapsulation alone accelerates folding by preventing the formation of reversible aggregates that limit the rate of the spontaneous folding reaction (Apetri and Horwich, 2008; Horwich et al., 2009).

To elucidate the mode of chaperonin action in accelerating folding, we characterized the kinetically trapped folding intermediate of DM-MBP and analyzed how GroEL/ES catalyzes its conversion to the native state. We show that encapsulation in the chaperonin cage accelerates folding not by blocking transient aggregation, but by mediating the progression of a collapsed, yet disordered folding intermediate toward the native state. A similar rate enhancement of folding can be achieved in the absence of chaperonin by introducing configurationally constraining, long-range disulfide bonds in the kinetically trapped intermediate. The effects of disulfide bonds and

chaperonin in accelerating folding are nonadditive. We conclude that protein confinement in the chaperonin cage has the capacity to reduce entropic folding barriers, thereby promoting the formation of native contacts. This function may define the uniquely essential role of GroEL/ES in protein folding.

RESULTS

Accelerated Folding by Chaperonin Independent of Aggregation Prevention

To investigate the mechanism by which the chaperonin promotes folding, we chose DM-MBP, containing mutations V8G and Y283D in MBP, as a model substrate. MBP consists of two domains, discontinuous in sequence, that are composed of α helices and β strands (Figure 1B) (Spurlino et al., 1991). The spontaneous refolding of DM-MBP is slow ($t_{1/2}$ ~30 min at 25°C), occurring with ~90% yield, but is accelerated up to 10-fold in the presence of GroEL/ES (under standard refolding conditions of 200 mM KCl, 60 mM GuHCl) (Figure 1C) (Tang et al., 2006). Spontaneous refolding is chloride sensitive (Apetri and Horwich, 2008) and is ~2-fold faster at 20 mM KCl or in the absence of GuHCl (Figure S1A available online). In contrast, the chaperonin-assisted folding is salt insensitive (Figure S1B). The rate enhancement of folding by GroEL/ES could reflect an active role of the chaperonin in catalyzing DM-MBP folding. Alternatively, the chaperonin may accelerate folding in a passive manner by preventing the formation of reversible aggregates that would reduce the folding rate but not the yield (Apetri and Horwich, 2008).

To distinguish between these possibilities, we first measured the rate and yield of DM-MBP folding over a wide concentration range (10 nM to 1.5 μM) by monitoring the increase in intrinsic tryptophan (Trp) fluorescence. These experiments were performed under standard refolding conditions. In accordance with our earlier observations (Tang et al., 2006), the rates and yields of spontaneous refolding were independent of protein concentration (Figure 1C and Figure S1C), strongly arguing against transient aggregation as a rate-limiting step. The accelerated rate of GroEL/ES-assisted folding was also concentration independent (Figure 1C and Figure S1D).

Next, we employed fluorescence correlation (FCS) and cross-correlation (FCCS) spectroscopy with fluorescent-labeled DM-MBP to assay aggregate formation directly. The rate of spontaneous folding of the labeled protein was similar to unlabeled DM-MBP and was accelerated ~6-fold by GroEL/ES (Sharma et al., 2008). To detect higher-order aggregates, FCS measurements were performed with a double cysteine mutant, DM-MBP(52–298), labeled with Atto532, by monitoring the decay of the autocorrelation function as a measure of the average diffusion time of particles through the probe volume. The diffusion coefficient of refolding DM-MBP (10 nM) (~54 $\mu m^2/s$) (Figure 1D), measured during the first 800 s upon dilution from denaturant, was similar to that of native DM-MBP (~58 $\mu m^2/s$). Importantly, the diffusion rate of the refolding, labeled DM-MBP remained unchanged in the presence of excess (1 or 2 μM) unlabeled, refolding DM-MBP, excluding the formation of large aggregates (Figure 1D). GroEL-bound DM-MBP (~800 kDa) was used as a control.

To test whether small aggregates, including dimers, formed during refolding, we performed FCCS experiments. DM-MBP labeled with either Atto532 or Atto647N was unfolded as a 1:1 mixture, and refolding initiated at a final concentration of ~10 nM. Assuming aggregation-limited folding kinetics, aggregates would be expected to be populated to ~75% during the first 250 s of refolding, corresponding to ~35% of particles containing both labels in case of exclusive dimer formation (see kinetic simulation in Figures S1E and S1F). However, dimeric or multimeric species were undetectable during refolding, based on the absence of a cross-correlation signal (Figure 1E). A mixture of the free dyes served as a negative control and a double-labeled DNA sample as a positive control (Figure 1E). Absence of aggregates during spontaneous DM-MBP refolding was also demonstrated by static and dynamic light-scattering measurements (Figures S2A and S2B).

The relationship between folding rate and aggregation was also explored for bacterial Rubisco, a GroEL substrate that is highly aggregation prone in a temperature-dependent manner (Brinker et al., 2001). At 15°C, the yield of spontaneous refolding decreased substantially with increasing concentration, due to aggregation (Figures S2C–S2G). Interestingly, the apparent rate of refolding was nevertheless concentration independent, indicating that the aggregates formed were irreversible. Folding was accelerated ~3-fold by GroEL/ES (Figures S2C and S2E). In summary, for both DM-MBP and Rubisco, the observed rate acceleration of folding must involve an active role of the chaperonin in modulating the intrinsic folding properties of these proteins and cannot be attributed to prevention of aggregation by a solely passive cage mechanism.

Slow Conversion of a Trapped Intermediate Limits Refolding

Having excluded transient aggregation as the rate-limiting step, it seemed likely that the formation of a monomeric, kinetically trapped folding intermediate(s) was responsible for the slow spontaneous refolding of DM-MBP. To define this species, we first recorded the denaturation-renaturation curves by Trp fluorescence and circular dichroism (CD) measurements after 12 hr of incubation in varying concentrations of denaturant. A prominent hysteresis effect was detected with an intermediate state being populated at 0.5–0.8 M GuHCl during the refolding phase, although the native state was thermodynamically stable up to ~0.7 M GuHCl (Figures 2A and 2B). Thus, this intermediate is kinetically trapped during refolding at intermediate denaturant concentration. The hysteresis effect was independent of protein concentration, as tested at 0.25 and 2 μM DM-MBP, and it was also observed with urea as denaturant in the absence of chloride salt (data not shown and Figures S3A and S3D). Interestingly, hysteresis was less pronounced with a single mutant of MBP containing only the Y283D substitution (SM-MBP), while no hysteresis was observed with wild-type MBP (WT-MBP) (Figures S3A–S3F), consistent with the relative order in folding rates of these proteins being DM-MBP < SM-MBP < WT-MBP (Tang et al., 2006). The kinetically trapped refolding intermediate of DM-MBP at 0.5 M GuHCl had molten globule-like properties. It contained only ~22% α-helical structure by CD and had a Trp fluorescence intensity as low as the unfolded protein (Figures

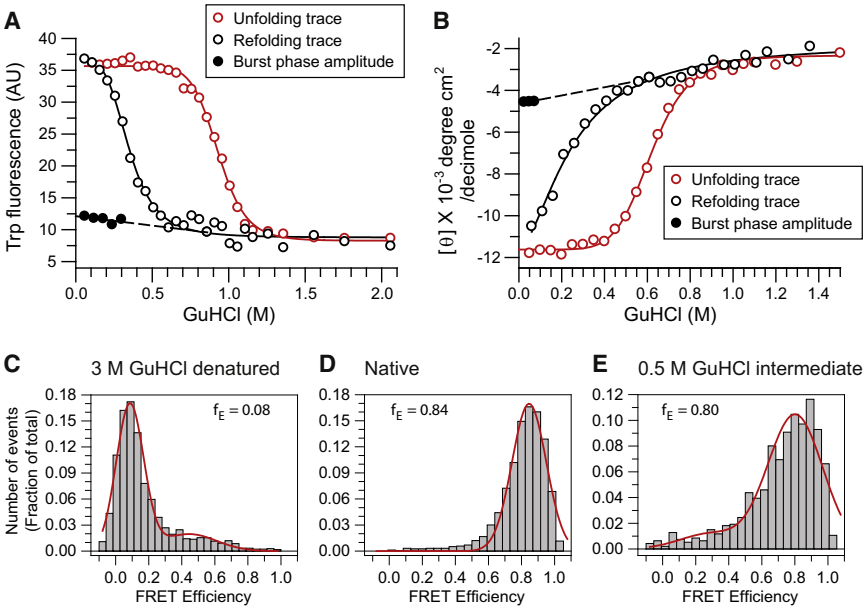

Figure 2. Characterization of a Kinetically Trapped Refolding Intermediate of DM-MBP

(A and B) GuHCl-dependent unfolding and refolding of DM-MBP (1 μM) was monitored by Trp fluorescence at 345 nm (A) and circular dichroism at 220 nm (B). Unfolding trace: native DM-MBP was incubated for 12 hr in buffer A containing ~60 mM to ~2 M GuHCl at 25°C. Refolding trace: DM-MBP (50 μM) was unfolded in 3 M GuHCl and then diluted 50-fold into buffer A containing different concentrations of GuHCl, followed by incubation for 12 hr at 25°C. Burst phase amplitudes were determined immediately on dilution from 3 M GuHCl. Representative data from at least two independent experiments.

(C–E) SpFRET analysis in solution of DM-MBP(52–298) double-labeled with Atto532 and Atto647N. (C) Denatured protein in 3 M GuHCl, (D) native protein, and (E) kinetically trapped folding intermediate in 0.5 M GuHCl are shown. Final protein concentration ~100 pM in buffer A containing GuHCl as indicated. Peak values of a Gaussian fit to the FRET efficiency distributions (f_E) are indicated. The shoulder of the f_E peaks in (C) and (E) were fitted with a second Gaussian to allow the correct determination of the peak f_E. Representative histograms from at least three independent measurements are shown.

See also Figure S3.

S3G and S3H), suggesting the absence of ordered tertiary structure. Spectroscopic analysis immediately upon dilution from 3 M to 60 mM GuHCl (burst phase amplitude) showed that a similar intermediate is also populated under refolding conditions (Figures 2A and 2B).

Single-pair FRET (spFRET) measurements in solution were next performed to analyze the compactness of the intermediate at 0.5 M GuHCl. DM-MBP(52–298) was double-labeled with Atto532 (position 52) as the fluorescence donor and Atto647N (position 298) as the acceptor (Sharma et al., 2008). These two positions are ~33 Å apart in the native structure (Figure 1B). The fully unfolded protein in 3 M GuHCl and the native protein showed narrow distributions of FRET efficiencies (f_E) with peak values of ~0.08 and ~0.84, respectively (Figures 2C and 2D) (Sharma et al., 2008). In comparison, the kinetically trapped refolding intermediate displayed a broader distribution centering on a f_E of ~0.80 (Figure 2E), suggesting that this species has an average compaction similar to that of the native protein but with a greater variability in structure, as demonstrated by the broader intramolecular distance distribution.

Pulsed hydrogen-deuterium (H/D) exchange measurements, coupled to mass spectrometry (MS), were next performed to further characterize this conformational ensemble (Figure 3A). The protonated and fully deuterated proteins were used as reference. Incorporation of deuterium by the kinetically trapped folding intermediate, generated by dilution from 3 M to 0.5 M GuHCl and incubation for 12 hr, corresponded to ~310 exchangeable amides (when corrected for ~10% back exchange and extrapolated to 100% D_2O during exchange) (Figure 3B). This was indistinguishable from the exchange properties of the fully denatured protein in 3 M GuHCl (~310 exchangeable amides) (Figure 3B), demonstrating the absence of stable secondary structure in the kinetically trapped intermediate. In contrast, WT-MBP under the same conditions displayed a structural stability similar to that of the native state at 60 mM GuHCl (~75 rapidly exchangeable amides) (Figure 3C), consistent with the absence of hysteresis between the unfolding and refolding curves (Figure S3C). Furthermore, pulsed H/D exchange of DM-MBP under refolding conditions (60 mM GuHCl) (Figure 3D) showed that an intermediate with exchange properties comparable to the kinetically trapped state at 0.5 M GuHCl was populated for more than 5 min during refolding, converting slowly to the native state (Figures 3E and 3B). A similar intermediate state was only transiently populated by WT-MBP (Figure 3F). Thus, the H/D exchange measurements together with the spectroscopic analysis demonstrate that DM-MBP populates under refolding conditions a kinetically trapped intermediate that is collapsed but lacks ordered structure. Structure formation within this dynamic intermediate appears to be rate limiting for folding, suggesting the existence of a significant entropic folding barrier.

Disulfide-Mediated Constraints Accelerate Spontaneous Refolding

Long-range disulfide bonds may serve to configurationally constrain flexible regions in folding intermediates, thereby entropically destabilizing them relative to the transition state and accelerating folding (Figure 4A) (Camacho and Thirumalai, 1995; Mamathambika and Bardwell, 2008). In addition, disulfide bonds can stabilize or destabilize the native state (Betz, 1993). To probe the entropic component of the folding barrier of DM-MBP, we engineered double-cysteine mutants with the

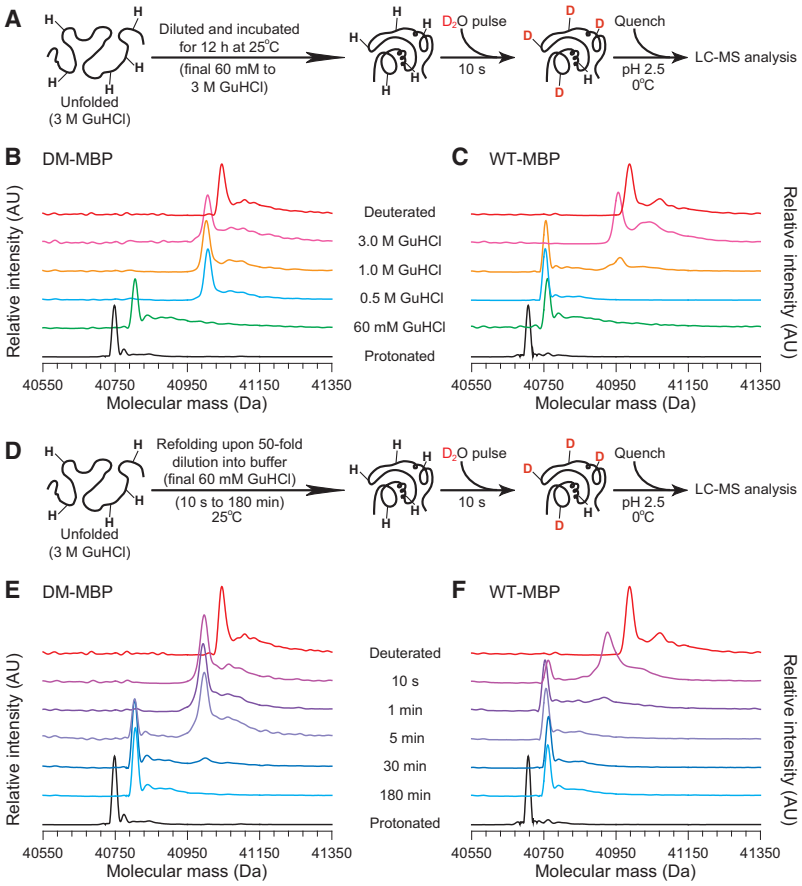

Figure 3. Dynamic Nature of Kinetically Trapped Refolding Intermediate Characterized by H/D Exchange

(A–C) Pulsed H/D exchange after incubation in different denaturant concentrations. Schematic representation of the experiment (A), deconvoluted mass spectra of DM-MBP (B), and WT-MBP (C) are shown. Global H/D exchange patterns as a function of denaturant monitored by ESI-QToF MS are shown. Proteins were diluted from 3 M GuHCl into buffer B with the final GuHCl concentrations indicated. After incubation for at least 12 hr, samples were subjected to a 10 s deuterium pulse. The native protonated and deuterated proteins are shown as reference.

(D–F) Pulsed H/D exchange under refolding conditions. Schematic representation of the experiment (D), deconvoluted mass spectra of DM-MBP (E), and WT-MBP (F) are shown. Global H/D exchange pattern as a function of refolding time is indicated. Refolding was initiated by dilution of denatured protein to a final concentration of 60 mM GuHCl in buffer B.

cysteines having appropriate positions and orientations for disulfide bond formation in the native state, while being far apart in the amino acid sequence. The N- and C-domain mutants, DM-MBP(18C–296C) and DM-MBP(184C–362C) (Figure 4B), readily formed the disulfide bond upon oxidation with $CuCl_2$ and bound maltose as efficiently as DM-MBP in the native state (Figures S4A and S4B). The oxidized (ox.) proteins refolded ~5-fold faster compared to the reduced (red.) proteins (Figures 4C and 4D and Figures S4C and S4D). To determine whether constraining the unfolded state was necessary for this effect, we took advantage of the finding that DM-MBP undergoes conformational collapse within milliseconds of initiating spontaneous folding (Sharma et al., 2008). When the reduced proteins were diluted from denaturant followed by addition of oxidizing agent, refolding was accelerated to the same extent as for the oxidized proteins (Figures 4C and 4D). Note that disulfide bond formation in the collapsed protein occurred within seconds of addition of oxidizing agent (Figures S4E–S4G). Conversely, refolding reverted to the slow rate of the reduced protein, when refolding was initiated from the oxidized protein and reducing agent (DTT) added after chain collapse (Figures 4C and 4D).

Assuming that the cysteines of DM-MBP(18C–296C) or DM-MBP(184C–362C) are proximal only in a certain subset of conformations of the collapsed state, disulfide formation would shift the distribution to more ordered conformations, in essence decreasing the chain entropy of the folding intermediate and destabilizing it with respect to the transition state (Figure 4A). Thus, the impact of disulfide bonds on folding may differ dependent on the exact regions of the protein that are restricted. Indeed, oxDM-MBP(18C–296C) refolded faster than oxDM-MBP(184C–362C) (Figures 4C and 4D). This difference in kinetics correlated with the absence of hysteresis in the unfolding-refolding curves of oxDM-MBP(18C–296C), whereas oxDM-MBP(184C–362C) preserved the hysteresis effect (Figures 4E and 4F and Figures S5A and S5B). H/D exchange measurements confirmed that at 0.5 M GuHCl, oxDM-MBP(18C–296C) was more structured than oxDM-MBP(184C–362C) (Figures S5C and S5D).

To estimate the possible effect of the disulfide bonds on the stability of the native state, we measured the rate of unfolding of the reduced and oxidized proteins. We found that the rate of unfolding was essentially unaffected by the disulfide bonds (Figure S5E and Table S1), consistent with the observation that the oxidized and reduced proteins showed similar stability toward denaturant (Figures 4E and 4F and Figures S5A and S5B). These results suggest that introducing disulfide bonds did not change the energy barrier from the native state to the transition state. Thus, it is plausible that the faster folding rate of the oxidized proteins is mainly due to a reduction of the energy barrier from the intermediate to the transition state (Figure 4A).

Chaperonin Cage Mimics Disulfide-Mediated Constraints

Having observed the effect of disulfides in accelerating folding, it seemed possible that confinement in the chaperonin cage may enhance folding speed by a similar mechanism. Alternatively, the chaperonin cage may accelerate folding by different means, in which case the presence of disulfides may have an additive effect. We used SR-EL, a single-ring mutant of GroEL (Weissman et al., 1996), to test how disulfide bond formation influences

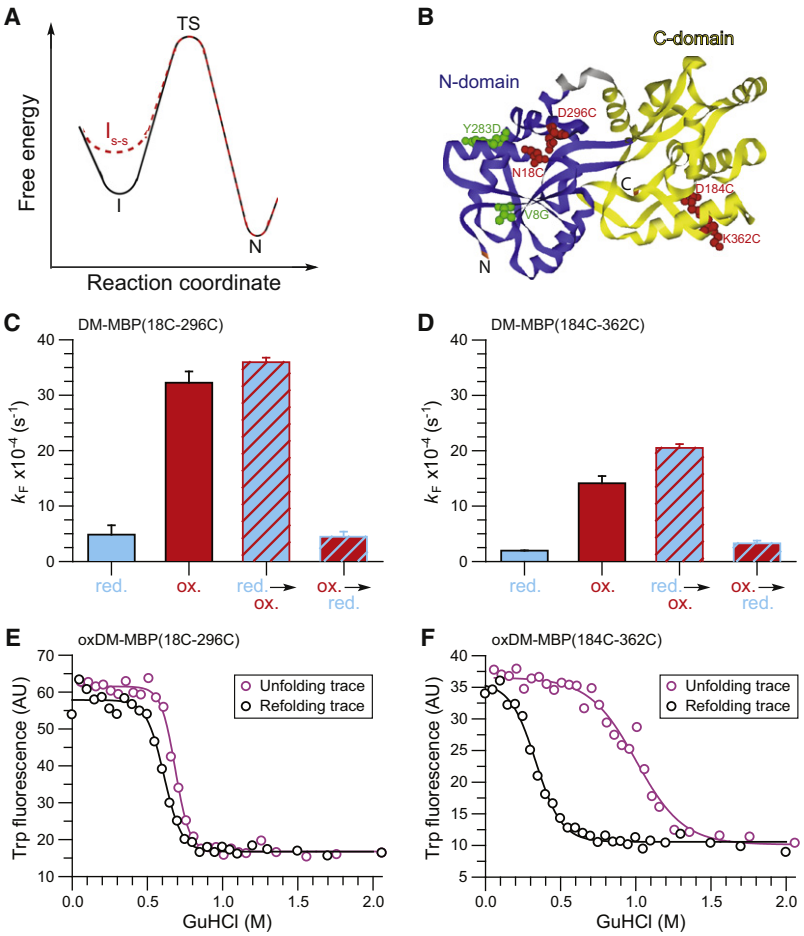

Figure 4. Disulfide Bridges Accelerate the Spontaneous Refolding of DM-MBP

(A) Free energy diagram illustrating the entropic destabilization of the kinetically trapped refolding intermediate (I) by disulfide-mediated structural constraints (I_{s-s}) relative to the folding transition state (TS), resulting in accelerated conversion to the native state (N).

(B) Ribbon diagram of the structure of MBP (see also Figure 1B), indicating the positions of DM-MBP mutations V8G and Y283D (green) and the cysteine pair mutations N18C-D296C and D184C-K362C (red). The two discontinuous domains are shown in blue (N-domain) and yellow (C-domain).

(C and D) Rates of spontaneous refolding of DM-MBP(18C–296C) (C) and DM-MBP(184C–362C) (D), 250 nM each in buffer A (final GuHCl 60 mM). Folding of reduced protein (red.) and oxidized protein (ox.), upon oxidizing the reduced protein 5 s after initiation of refolding (red. → ox.) or upon reducing the oxidized protein 5 s after initiation of refolding (ox. → red.). Refolding was followed by monitoring Trp fluorescence as in Figure 1C. Standard deviation from three independent measurements.

(E and F) GuHCl-dependent unfolding and refolding of oxidized (ox) DM-MBP(18C–298C) (E) and oxDM-MBP(184C–362C) (F) were monitored by Trp fluorescence as in Figure 2A.

See also Figure S4, Figure S5, and Table S1.

folding within the chaperonin cage. SR-EL undergoes only a single round of ATP hydrolysis upon GroES binding, resulting in stable substrate encapsulation in low-salt buffer (Figure 5A) (Hayer-Hartl et al., 1996). Under these conditions (20 mM KCl/60 mM GuHCl), oxDM-MBP(18C–296C) and oxDM-MBP(184C–362C) refolded at similar rates. SR-EL/ES accelerated the folding of both oxidized proteins ~1.5 times beyond their spontaneous refolding rates (Figures 5B and 5C). Notably, the rate of SR-EL/ES-assisted folding was independent of the presence of the disulfide bonds.

The finding that SR-EL/ES accelerated the folding of the oxidized proteins beyond their spontaneous folding rates would be consistent with the chaperonin cavity exerting a global confinement effect, whereas disulfide bond-mediated structural constraints act more locally. To examine this possibility, we constructed a DM-MBP variant, DM-MBP(4C), combining both the 18C-296C and 184C-362C disulfide bonds. Strikingly, the spontaneous folding of oxDM-MBP(4C) was fully accelerated to the rate of chaperonin-assisted folding (Figure 5D). As in the case of the single disulfide bonds, the rate of assisted folding was the same for the oxidized and reduced proteins (Figure 5D). Thus, the effect of constraining both domains of DM-MBP is comparable to the global compaction exerted by the chaperonin.

To investigate further whether long-range disulfide bonds energetically mimic the confinement by the chaperonin cage, we analyzed the temperature dependence of the folding rates. The spontaneous refolding of DM-MBP, redDM-MBP(18C–296C), and redDM-MBP(4C) proved to be relatively insensitive to temperature variation between 15°C and 25°C (Figures 5E–5G), consistent with a large entropic folding barrier (Bicout and Szabo, 2000). Based on the apparent two-state behavior of the folding reaction, in which the kinetically trapped intermediate and the native state are the main populated species (Figure 3 and Figure 4A), we used the temperature dependence of the folding rate to provide an approximate estimate of the enthalpic and entropic contributions to the folding energy barrier (Table S2). As expected, the activation barrier for the spontaneous folding of the reduced proteins was mostly entropic in nature. In contrast, the folding rate of the oxidized proteins showed a pronounced, positive temperature dependence (Figure 5E), indicating that the activation barrier has gained a significant enthalpic component and the entropic contribution is largely reduced (Table S2). Strikingly, the SR-EL/ES-assisted folding of DM-MBP and the reduced cysteine mutants displayed a similar positive temperature dependence (Figures 5E–5G), suggesting a strongly reduced entropic folding barrier (Table S2). Thus, the spontaneous folding of the oxidized proteins and the chaperonin-assisted folding of the reduced proteins have similar rate-limiting steps, consistent with a common mechanism of accelerated folding by entropic confinement. The enthalpic component of the activation barrier may reflect side-chain friction during folding, resulting either from

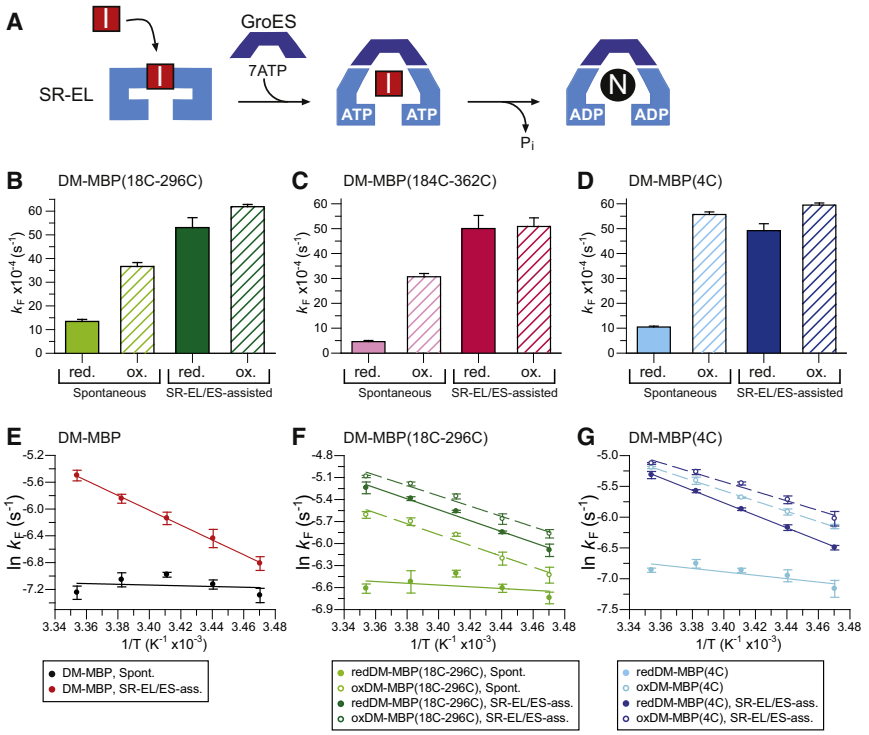

Figure 5. Chaperonin-Assisted Folding Is Insensitive to Disulfide Formation

(A) Protein folding in the SR-EL/ES cage upon a single round of encapsulation of folding intermediate (I). Due to the lack of a second ring, the native protein (N) remains encapsulated.

(B–D) Rates of spontaneous and assisted refolding of DM-MBP(18C–296C) (B), DM-MBP(184C–362C) (C), and DM-MBP(4C) (D) in the reduced (red.) and oxidized states (ox.). Refolding was performed at 250 nM DM-MBP in buffer B (see Experimental Procedures). No folding was observed in the presence of SR-EL when GroES was absent (data not shown). Standard deviation from three independent measurements.

(E–G) Arrhenius plots of spontaneous and SR-EL/ES-assisted refolding of DM-MBP (E), reduced and oxidized DM-MBP(18C–296C) (F), and DM-MBP(4C) (G). Refolding was performed at 250 nM DM-MBP in buffer B. Temperature was varied from 15°C–25°C. Standard deviation from three independent measurements.

See also Figure S4, Figure S5, Table S1, and Table S2.

disulfide-mediated constraints or steric restrictions imposed by the chaperonin cage.

Charge Clusters in the Cage Wall as an Active Principle in Promoting Folding

The wall of the GroEL/ES cage is highly charged, exhibiting a net charge of minus 42 (147 positively and 189 negatively charged residues) (Xu et al., 1997). To determine whether these charge properties are important in promoting DM-MBP folding, we took advantage of a mutant of SR-EL, SR-KKK2 (Tang et al., 2006), which has a cavity net charge of zero due to mutation of three conserved, negatively charged residues per subunit (D359, D361, E363) to lysines (Figure 6A). As shown previously, SR-KKK2 binds and encapsulates DM-MBP as efficiently as SR-EL but is unable to accelerate its folding (Figures S6A and S6B), whereas the rate of WT-MBP folding is essentially unaffected (Tang et al., 2006). This suggests that the KKK2 mutant may have lost the ability to reduce the entropic barrier of DM-MBP folding, in which case the rate-limiting step of folding inside the mutant chaperonin may be similar to that of spontaneous folding.

To test this possibility, we first recorded the temperature dependence of SR-KKK2/ES-assisted folding. (Note that SR-EL and SR-KKK2 have similar ATPase rates and undergo only a single round of ATP hydrolysis upon GroES binding.) In contrast to SR-EL/ES-mediated folding, the SR-KKK2/ES-assisted folding of DM-MBP was temperature independent, similar to spontaneous folding (Figure 6B). Introducing disulfide bonds restored the positive temperature dependence of folding, as shown for oxDM-MBP(18C–296C) (Figure 6B). Thus, SR-KKK2 seems to have lost (or significantly reduced) the ability to entropically destabilize the DM-MBP folding intermediate (Table S2).

To corroborate this conclusion, we analyzed the folding reactions under various physical conditions, including the effect of low denaturant, which may increase the flexibility of the kinetically trapped intermediate, thereby decelerating folding. Indeed, the rate of spontaneous and SR-KKK2/ES-assisted folding of DM-MBP decreased with GuHCl (15–60 mM) (Figure 6C). In contrast, the SR-EL/ES-assisted folding rate was independent of denaturant (Figure 6C), consistent with the ability of the wild-type chaperonin to promote structure formation in the intermediate. Next, we tested the influence of trimethylamine *N*-oxide (TMAO) on folding, an osmolyte known to reduce structural flexibility in proteins (Qu and Bolen, 2003), presumably via the enhancement of water structure (Zou et al., 2002). The rate of spontaneous and SR-KKK2/ES-assisted folding showed a positive dependence on TMAO concentration (Figure 6D), whereas the SR-EL/ES-assisted folding remained essentially unchanged (Figure 6D). This suggests that the wild-type chaperonin mimics the effect of TMAO, consistent with the proposal that the charged lining of the cage may promote protein compaction by an ordering effect on water structure (England and Pande, 2008). Together, these results provide evidence that by removing its negative net charge, the chaperonin cavity is converted from an active to a largely passive folding environment.

DISCUSSION

Our analysis of spontaneous and GroEL/ES-assisted folding of DM-MBP provides insight into the conformational properties of a protein that determine its chaperonin dependence. We have

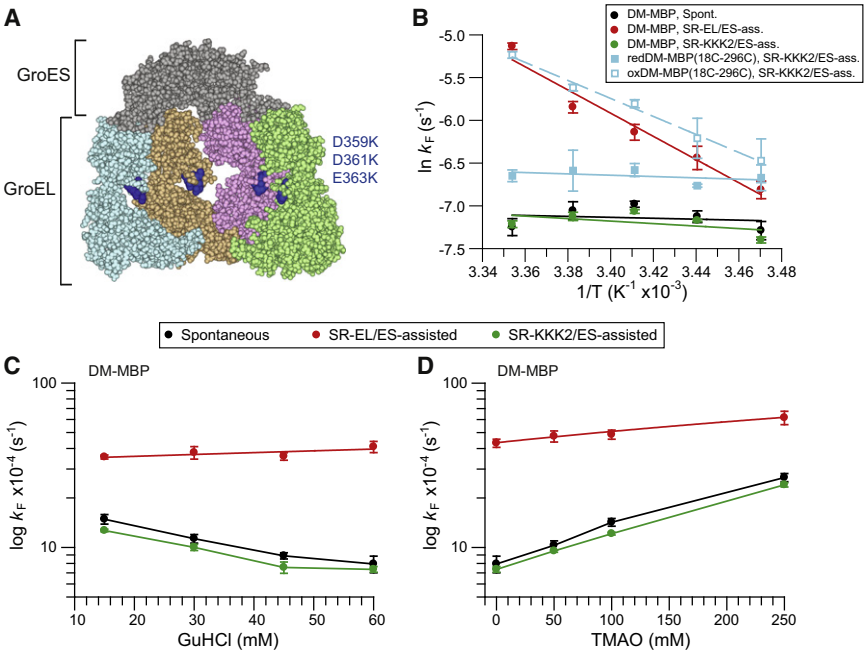

Figure 6. Cavity Wall Charges Are Necessary for Accelerated Chaperonin-Assisted Folding

(A) Space-filling model of four subunits of the GroEL/ES-$(ADP)_7$ complex (Xu et al., 1997; PDB 1AON, DS ViewerPro) offering a view into the chaperonin folding cage. The negatively charged residues mutated in SR-KKK2 (D359K; D361K; E363K) are highlighted in blue.

(B) Temperature dependence of spontaneous and assisted folding by SR-EL/ES or SR-KKK2/ES of DM-MBP and reduced and oxidized DM-MBP(18C–296C). Refolding was measured as in Figure 5E (data from Figure 5E are shown for comparison). Standard deviation from three independent measurements.

(C and D) Rates of spontaneous and assisted refolding of DM-MBP at varying concentrations of GuHCl (C) and TMAO (D). Refolding was performed as above, either spontaneous or assisted by SR-EL/ES or SR-KKK2/ES as indicated. Standard deviation from three independent measurements.

See also Figure S6 and Table S2.

shown that DM-MBP, a protein with complex two-domain topology, folds slowly due to the formation of a kinetically trapped intermediate that is collapsed but structurally disordered. Introducing native, long-range disulfide bonds reduces the chain entropy of the trapped intermediate and accelerates folding several-fold (Figure 7A). Strikingly, confinement of the reduced protein in the GroEL/ES cage closely mimics the accelerating effect of the constraining disulfides (Figure 7B). We propose that the capacity of the chaperonin cage to overcome entropic barriers in the folding energy landscape (Figure 7C) serves to promote the folding of a restricted set of obligate substrates and may also endow GroEL/ES with the ability to buffer mutations that kinetically disable the folding pathways of otherwise chaperonin-independent proteins (Tokuriki and Tawfik, 2009).

Passive versus Active Chaperonin Mechanisms

In the present study, we have employed a range of biophysical techniques to rule out transient aggregation as the cause of slow spontaneous folding for the model substrate DM-MBP. We find that DM-MBP has a substantially lower aggregation propensity than authentic GroEL substrates, while resembling the latter with regard to fold topology and the inability to interact productively with other chaperones, such as the Hsp70 system (DnaK/DnaJ) (Kerner et al., 2005; Tang et al., 2006). Based on the concentration independence of the folding rate over a wide range (10 nM to 1.5 μM) and the absence of multimers by FCS, FCCS, and light scattering, we conclude that under the experimental conditions in vitro, spontaneous DM-MBP refolding is kinetically limited by an intrinsic barrier, not aggregation (Figures 1C and 1D and Figures S1C and S1D). Moreover, we demonstrate that in the case of the GroEL-dependent protein Rubisco, aggregation is irreversible and affects only the yield but not the rate of folding. Thus, the observed rate enhancement of DM-MBP and Rubisco folding necessitates an active mechanism of the chaperonin in promoting folding. This mechanism operates synergistically with the capacity of the GroEL/ES chamber to prevent aggregation by substrate encapsulation (Brinker et al., 2001).

Basis of Slow DM-MBP Folding

The folding of larger, topologically complex proteins is often slow. The native states of such proteins are stabilized to a significant extent by long-range contacts, the formation of which can be more effectively counteracted by conformational entropy than that of local contacts (Plaxco et al., 1998). In the case of DM-MBP, slow folding is due to a dominantly populated, kinetically trapped intermediate that is separated from the native state by a significant free energy barrier. This barrier has a large entropic component, based on the temperature independence of the folding rate (Table S2). Population of the kinetically trapped intermediate causes a prominent hysteresis in the unfolding/refolding curves. The intermediate (in the presence of 0.5 M GuHCl or immediately upon removal from denaturant) is collapsed but has a broader intramolecular distance distribution than the native state, as determined by spFRET, and is structurally disordered and dynamic based on its CD, Trp fluorescence, and H/D exchange properties (Figure 2, Figure 3, and Figures S3G and S3H). The lack of ordered structure suggests that this kinetically trapped intermediate is not significantly stabilized by native or non-native side-chain packing, thus imposing a large entropic barrier to folding.

This model was tested by introducing configurational constraints mediated by disulfide bonds between residues that are juxtaposed in the native structure but far apart along the sequence (Figure 7A). The two domains of DM-MBP are discontiguous in sequence (Figure 4B), suggesting that they are structurally interdependent, and formation of native contacts in the N-domain, carrying the two mutations V8G and Y283D, has

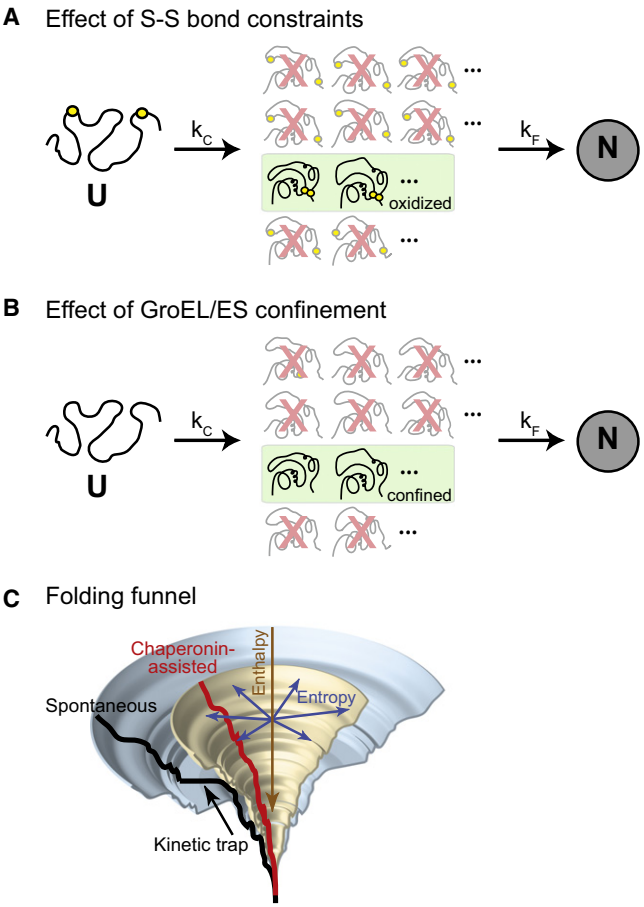

Figure 7. Models for Accelerated Folding by Entropic Destabilization of Kinetically Trapped Refolding Intermediate

(A and B) Schematic representations of refolding of DM-MBP with disulfide bridge-mediated restriction of conformational flexibility (A) and confinement by chaperonin (B). Upon dilution from denaturant, unfolded DM-MBP (U) undergoes rapid collapse (k_C) to an ensemble of intermediate states that must cross an entropic barrier for folding (k_F) to the native state (N). Introducing long-range disulfide bonds reduces this barrier by conformationally restricting the ensemble of kinetically trapped states to more ordered states, resulting in accelerated folding. Confinement of DM-MBP inside the chaperonin cage mimics the effect of disulfide bonds by eliminating more disordered states.

(C) The hypothetical folding funnel of DM-MBP is shown in light blue with the vertical axis denoting enthalpy (arrow to lower enthalpy) and the radial plane denoting entropy of the folding intermediates (arrow to higher entropy). The large flat area in the folding funnel denotes the kinetically trapped intermediate that is separated from the native state through an entropic barrier. This is modified inside the chaperonin cage (light orange funnel), resulting in a more downhill funnel without the presence of prominent isoenthalpic regions representing entropically stabilized intermediate states.

been shown to be rate limiting for folding (Chun et al., 1993). Indeed, introducing a long-range disulfide bond in the N- or C-domain accelerated folding several-fold (Figures 4C and 4D and Figures 5B and 5C), without stabilizing the native state (Figures S5A and S5B and Table S1). Combining the two disulfide bonds had an approximately additive effect on folding rate (Figures 5B–5D). Notably, acceleration of folding was also observed when the disulfide bonds were allowed to form only after the collapse reaction (Figures 4C and 4D), suggesting that the respective residues are transiently proximal in the kinetically trapped intermediate. Constraining already proximal residues should accelerate folding only if substantial flexibility exists around these regions. This is consistent with the view that for proteins with complex topology, reducing chain entropy by stabilizing long-range, native contacts may accelerate the search of the favorable energetic interactions that define the transition state (Bartlett and Radford, 2009; Plaxco et al., 1998; Vendruscolo et al., 2003; Wallin and Chan, 2006). Introducing disulfide bonds rendered the folding rate of DM-MBP temperature dependent, reflecting an increased enthalpic component and a strongly reduced entropic component of the folding barrier (Table S2).

Mechanism of Accelerated Folding by Chaperonin

Our results argue that the chaperonin cage limits the conformational entropy of the kinetically trapped folding intermediate of DM-MBP in a way resembling the entropic constraints afforded by long-range disulfide bonds (Figure 7). Notably, the accelerating effects of disulfide bonds and of chaperonin on folding were nonadditive (Figures 5B–5D). Global confinement in the chaperonin cage accelerated folding more efficiently than the single disulfide bonds but did not enhance the faster folding rate obtained by combining the two disulfides. This is consistent with disulfide-mediated constraints and confinement by the chaperonin modulating the thermodynamic parameters of the folding reaction in a similar way. The finding that both chaperonin-assisted and disulfide-mediated folding have a positive temperature dependence of folding rate strongly supports the assumption of a common, underlying principle in reducing the entropic activation barrier of the folding reaction.

The ability of GroEL/ES to accelerate folding was markedly dependent on the negative charge character of the cage wall. Removal of the net-negative charge rendered the cavity unable to accelerate folding but did not interfere with the rapid folding of the oxidized proteins, suggesting that the mutant cage is providing DM-MBP with a more passive folding environment. These findings are consistent with recent theoretical considerations that the charged surface may induce ordered water structure, with the resulting increase in the density of water facilitating folding by enhancing the hydrophobic effect and thus promoting global protein compaction (England and Pande, 2008; Lucent et al., 2007). Importantly, this change in solvent behavior can only take effect when the folding protein is brought into close proximity to the cavity wall. In accordance with theory and simulation (Baumketner et al., 2003; Hayer-Hartl and Minton, 2006), decreasing the size of the chaperonin cage has been shown to accelerate the folding of smaller GroEL substrates (Tang et al., 2006, 2008), suggesting that charge effects from the cavity wall and geometric confinement act in concert to smooth the folding energy landscape (Figure 7C).

The cage-mediated acceleration of folding by GroEL/ES described here is mechanistically independent of repeated cycles of substrate binding and release from the hydrophobic apical domains of GroEL. Substrate cycling has been proposed to accelerate folding by iteratively unfolding kinetically trapped intermediates stabilized by non-native interactions, allowing

repartitioning to a productive folding pathway upon release (iterative annealing) (Shtilerman et al., 1999; Thirumalai and Lorimer, 2001). Indeed, ATP-dependent apical domain movements can cause local structural expansion (Lin et al., 2008; Sharma et al., 2008), but in the case of DM-MBP and Rubisco, such "forced" unfolding was dispensable for folding acceleration (Brinker et al., 2001; Sharma et al., 2008). This may be readily explained by our finding that the kinetically trapped folding intermediate of DM-MBP is highly disordered and thus unlikely to contain strong non-native contacts. Consequently, further unfolding would not circumvent formation of the folding trap.

Biological Significance

The GroEL/ES system is essential under all growth conditions and is normally utilized by ~10% of newly synthesized cytosolic proteins, including ~80 proteins that are predicted to be chaperonin dependent for folding (Ewalt et al., 1997; Houry et al., 1999; Kerner et al., 2005). Like DM-MBP, these proteins have complex alpha and beta domain topologies and are thought to populate kinetically trapped folding intermediates (Kerner et al., 2005). In view of the fact that cells contain multiple, partially redundant chaperone systems for aggregation prevention, the ability to actively promote the folding of such intermediates would explain the uniquely essential role of the chaperonin cages. On the other hand, the conspicuous absence of chaperonins from oxidizing cellular compartments correlates with the role of disulfide bond formation in providing an alternative mechanism to lower entropic folding barriers.

EXPERIMENTAL PROCEDURES

Proteins

Chaperonin, MBP, and Rubisco proteins were purified as described in (Brinker et al., 2001; Sharma et al., 2008; Tang et al., 2006) (see Extended Experimental Procedures).

MBP Refolding

Generally, DM-MBP and its cysteine mutants (25 μM) (reduced or oxidized) were denatured in 6 M GuHCl with or without 5 mM DTT and refolded at 25°C upon 100-fold dilution into buffer A (20 mM Tris, pH 7.5, 200 mM KCl, 5 mM $Mg(OAc)_2$) or into buffer B (20 mM Tris, pH 7.5, 20 mM KCl, 5 mM $Mg(OAc)_2$) in the absence or presence of chaperonins at the concentrations indicated in the figure legends (see Extended Experimental Procedures for details). Refolding experiments were also carried out at different final GuHCl concentrations, at different TMAO concentrations, and at different temperatures when indicated. Refolding was monitored (295 nm excitation, 345 nm emission) by following the increase in intrinsic Trp fluorescence on a Fluorolog spectrofluorometer (FL3-22, Spex) for DM-MBP concentrations of 10 nM to 2 μM (Tang et al., 2006), taking advantage of the absence of Trp residues in GroEL, SR-EL, and GroES (Martin et al., 1991). Excitation (0.5 or 1 nm) and emission slit widths (5 or 10 nm) as well as shutter speed were adjusted at different protein concentrations to avoid photobleaching. Refolding and unfolding experiments, monitored by CD and Trp fluorescence, were performed as described in the Extended Experimental Procedures. Note that the spontaneous and SR-KKK2/ES-assisted folding rates are slowed by the presence of chloride salt, whereas wild-type chaperonin-mediated folding is salt independent (see Figure S1A, Figure S1B, and Figure S6C).

Single-pair FRET, FCS, and FCCS Experiments

Fluorescence correlation spectroscopy (FCS), fluorescence cross-correlation spectroscopy (FCCS), and single-pair FRET (spFRET) experiments were performed using pulsed interleaved excitation (Muller et al., 2005) either on a homebuilt confocal microscope system or on a Microtime 200 instrument (PicoQuant GmbH). FCS and FCCS were used to investigate the oligomeric state of DM-MBP during spontaneous refolding. The conformation of the DM-MBP was measured by spFRET. See Extended Experimental Procedures for further details.

Hydrogen/Deuterium Exchange Pulse Labeling

MBP protein (100 μM) was unfolded in 3 M GuHCl. Samples were diluted 50-fold and incubated for at least 12 hr at final GuHCl concentrations of 60 mM to 3 M in buffer B. Pulse H/D exchange was performed by diluting MBP protein (2 pmol/μl; 50 μl) 1:10 into deuterated 20 mM Tris DCl, 20 mM KCl, 5 mM $Mg(OAc)_2$, D_2O, pH 7.5 (pH meter reading uncorrected for isotope effect; Connelly et al., 1993) at 25°C. MBP samples containing GuHCl were labeled with buffer containing an equivalent concentration of GuDCl. The exchange reaction was quenched after 10 s to pH ~2.5 by addition of 200 μl ice-cold 600 mM sodium phosphate buffer, pH 2.4. Quenched samples (700 μl) were immediately concentrated to 100 μl using Vivaspin spin columns at ~0°C for 5 min. Samples were flash frozen in liquid nitrogen and stored at −80°C and analyzed by MS within 2 days as described in the Extended Experimental Procedures.

SUPPLEMENTAL INFORMATION

Supplemental information includes Extended Experimental Procedures, six figures, and two tables and can be found with this article online at doi:10.1016/j.cell.2010.05.027.

ACKNOWLEDGMENTS

We thank J.R. Engen for sharing with us the blueprints of his home-built microflow HPLC system and A.R. Lange for technical assistance. We gratefully acknowledge financial support from Deutsche Forschungsgemeinschaft (SFB 596 to F.U.H. and M.H.-H., and SFB 749 to D.C.L.), the Ludwig-Maximilians-University Munich (LMUInnovativ BioImaging Network), Nanosystems Initiative Munich (NIM), the Ernst-Jung Foundation, and the Körber Foundation.

Received: November 30, 2009
Revised: March 21, 2010
Accepted: April 23, 2010
Published: July 8, 2010

REFERENCES

Apetri, A.C., and Horwich, A.L. (2008). Chaperonin chamber accelerates protein folding through passive action of preventing aggregation. Proc. Natl. Acad. Sci. USA *105*, 17351–17355.

Bartlett, A.I., and Radford, S.E. (2009). An expanding arsenal of experimental methods yields an explosion of insights into protein folding mechanisms. Nat. Struct. Mol. Biol. *16*, 582–588.

Baumketner, A., Jewett, A., and Shea, J.E. (2003). Effects of confinement in chaperonin assisted protein folding: Rate enhancement by decreasing the roughness of the folding energy landscape. J. Mol. Biol. *332*, 701–713.

Bicout, D.J., and Szabo, A. (2000). Entropic barriers, transition states, funnels, and exponential protein folding kinetics: A simple model. Protein Sci. *9*, 452–465.

Betz, S.F. (1993). Disulfide bonds and the stability of globular proteins. Protein Sci. *2*, 1551–1558.

Brinker, A., Pfeifer, G., Kerner, M.J., Naylor, D.J., Hartl, F.U., and Hayer-Hartl, M. (2001). Dual function of protein confinement in chaperonin-assisted protein folding. Cell *107*, 223–233.

Camacho, C.J., and Thirumalai, D. (1995). Modeling the role of disulfide bonds in protein folding - entropic barriers and pathways. Proteins *22*, 27–40.

Chun, S.Y., Strobel, S., Bassford, P., Jr., and Randall, L.L. (1993). Folding of maltose-binding protein. Evidence for the identity of the rate-determining step in vivo and in vitro. J. Biol. Chem. *268*, 20855–20862.

Connelly, G.P., Bai, Y., Jeng, M.F., and Englander, S.W. (1993). Isotope effects in peptide group hydrogen exchange. Proteins *17*, 87–92.

England, J.L., and Pande, V.S. (2008). Potential for modulation of the hydrophobic effect inside chaperonins. Biophys. J. *95*, 3391–3399.

Ewalt, K.L., Hendrick, J.P., Houry, W.A., and Hartl, F.U. (1997). In vivo observation of polypeptide flux through the bacterial chaperonin system. Cell *90*, 491–500.

Frydman, J. (2001). Folding of newly translated proteins in vivo: The role of molecular chaperones. Annu. Rev. Biochem. *70*, 603–647.

Hartl, F.U., and Hayer-Hartl, M. (2002). Molecular chaperones in the cytosol: from nascent chain to folded protein. Science *295*, 1852–1858.

Hartl, F.U., and Hayer-Hartl, M. (2009). Converging concepts of protein folding in vitro and in vivo. Nat. Struct. Mol. Biol. *16*, 574–581.

Hayer-Hartl, M., and Minton, A.P. (2006). A simple semiempirical model for the effect of molecular confinement upon the rate of protein folding. Biochemistry *45*, 13356–13360.

Hayer-Hartl, M.K., Weber, F., and Hartl, F.U. (1996). Mechanism of chaperonin action: GroES binding and release can drive GroEL-mediated protein folding in the absence of ATP hydrolysis. EMBO J. *15*, 6111–6121.

Horwich, A.L., Apetri, A.C., and Fenton, W.A. (2009). The GroEL/GroES cis cavity as a passive anti-aggregation device. FEBS Lett. *583*, 2654–2662.

Houry, W.A., Frishman, D., Eckerskorn, C., Lottspeich, F., and Hartl, F.U. (1999). Identification of in vivo substrates of the chaperonin GroEL. Nature *402*, 147–154.

Jewett, A.I., and Shea, J.-E. (2010). Reconciling theories of chaperonin accelerated folding with experimental evidence. Cell. Mol. Life Sci. *67*, 255–276.

Kerner, M.J., Naylor, D.J., Ishihama, Y., Maier, T., Chang, H.C., Stines, A.P., Georgopoulos, C., Frishman, D., Hayer-Hartl, M., Mann, M., et al. (2005). Proteome-wide analysis of chaperonin-dependent protein folding in *Escherichia coli*. Cell *122*, 209–220.

Lin, Z., Madan, D., and Rye, H.S. (2008). GroEL stimulates protein folding through forced unfolding. Nat. Struct. Mol. Biol. *15*, 303–311.

Lucent, D., Vishal, V., and Pande, V.S. (2007). Protein folding under confinement: a role for solvent. Proc. Natl. Acad. Sci. USA *104*, 10430–10434.

Mamathambika, B.S., and Bardwell, J.C. (2008). Disulfide-linked protein folding pathways. Annu. Rev. Cell Dev. Biol. *24*, 211–235.

Martin, J., Langer, T., Boteva, R., Schramel, A., Horwich, A.L., and Hartl, F.U. (1991). Chaperonin-mediated protein folding at the surface of GroEL through a 'molten globule'-like intermediate. Nature *352*, 36–42.

Mayhew, M., Da Silva, A.C.R., Martin, J., Erdjument-bromage, H., Tempst, P., and Hartl, F.U. (1996). Protein folding in the central cavity of the GroEL-GroES chaperonin complex. Nature *379*, 420–426.

Muller, B.K., Zaychikov, E., Brauchle, C., and Lamb, D.C. (2005). Pulsed interleaved excitation. Biophys. J. *89*, 3508–3522.

Plaxco, K.W., Simons, K.T., and Baker, D. (1998). Contact order, transition state placement and the refolding rates of single domain proteins. J. Mol. Biol. *277*, 985–994.

Qu, Y.X., and Bolen, D.W. (2003). Hydrogen exchange kinetics of RNase A and the urea: TMAO paradigm. Biochemistry *42*, 5837–5849.

Sharma, S., Chakraborty, K., Mueller, B.K., Astola, N., Tang, Y.C., Lamb, D.C., Hayer-Hartl, M., and Hartl, F.U. (2008). Monitoring protein conformation along the pathway of chaperonin-assisted folding. Cell *133*, 142–153.

Shtilerman, M., Lorimer, G.H., and Englander, S.W. (1999). Chaperonin function: Folding by forced unfolding. Science *284*, 822–825.

Spurlino, J.C., Lu, G.Y., and Quiocho, F.A. (1991). The 2.3-A resolution structure of the maltose- or maltodextrin-binding protein, a primary receptor of bacterial active transport and chemotaxis. J. Biol. Chem. *266*, 5202–5219.

Tang, Y.C., Chang, H.C., Roeben, A., Wischnewski, D., Wischnewski, N., Kerner, M.J., Hartl, F.U., and Hayer-Hartl, M. (2006). Structural features of the GroEL-GroES nano-cage required for rapid folding of encapsulated protein. Cell *125*, 903–914.

Tang, Y.C., Chang, H.C., Chakraborty, K., Hartl, F.U., and Hayer-Hartl, M. (2008). Essential role of the chaperonin folding compartment in vivo. EMBO J. *27*, 1458–1468.

Thirumalai, D., and Lorimer, G.H. (2001). Chaperonin-mediated protein folding. Annu. Rev. Biophys. Biomol. Struct. *30*, 245–269.

Tokuriki, N., and Tawfik, D.S. (2009). Chaperonin overexpression promotes genetic variation and enzyme evolution. Nature *459*, 668–671.

Vendruscolo, M., Paci, E., Karplus, M., and Dobson, C.M. (2003). Structures and relative free energies of partially folded states of proteins. Proc. Natl. Acad. Sci. USA *100*, 14817–14821.

Wallin, S., and Chan, H.S. (2006). Conformational entropic barriers in topology-dependent protein folding: perspectives from a simple native-centric polymer model. J. Phys. Condes. Matter *18*, S307–S328.

Weissman, J.S., Rye, H.S., Fenton, W.A., Beechem, J.M., and Horwich, A.L. (1996). Characterization of the active intermediate of a GroEL-GroES-mediated protein folding reaction. Cell *84*, 481–490.

Xu, Z.H., Horwich, A.L., and Sigler, P.B. (1997). The crystal structure of the asymmetric GroEL-GroES-(ADP)7 chaperonin complex. Nature *388*, 741–749.

Zou, Q., Bennion, B.J., Daggett, V., and Murphy, K.P. (2002). The molecular mechanism of stabilization of proteins by TMAO and its ability to counteract the effects of urea. J. Am. Chem. Soc. *124*, 1192–1202.

Cell

EXTENDED EXPERIMENTAL PROCEDURES

Proteins and DM-MBP Constructs

The *E. coli* proteins GroEL, GroEL(D87K), GroES, SR-EL, SR-KKK2, Rubisco from Rhodospirillum rubrum and Rubisco mutant K168E, WT-MBP and DM-MBP proteins were purified as described previously (Brinker et al., 2001; Sharma et al., 2008; Tang et al., 2006). Double cysteine and tetra cysteine DM-MBP variants, pCH-DM-MBP(N18C-D296C), pCH-DM-MBP(D184C-K362C) and pCH-DM-MBP(N18C-D296C-D184C-K362C), were generated by site-directed mutagenesis to analyze disulfide mediated refolding. Protein concentrations were determined spectrophotometrically.

Unfolding and Refolding Curves of DM-MBP

Refolding experiments were carried out by 50-fold dilution of DM-MBP proteins from buffer A/3M GuHCl into buffer A containing ~60 mM to ~2 M GuHCl (refolding/unfolding was also performed with urea as the denaturant). Unfolding experiments were carried out by 50-fold dilution of native DM-MBP proteins into GuHCl-containing buffer A. Samples were incubated for 12 hr at 25°C. The fraction of folded protein was determined at 25°C by monitoring intrinsic Trp fluorescence at 345 nm and Far-UV circular dichroism (CD) at 220 nm (Jasco J-715 spectropolarimeter equipped with Peltier-thermostat at 25°C using 0.1 or 0.2 cm cuvettes). The percentages of secondary structure were determined using Contin software (Sreerama and Woody, 2004).

Refolding of Reduced and Oxidized DM-MBP

Refolding of DM-MBP cysteine mutants under reducing conditions was performed in the presence of 5 mM DTT. Oxidized cysteine mutants were prepared by removing DTT from native protein by Micro-Biospin 6 columns (Biorad) equilibrated with buffer A or B and oxidizing it for 1 hr at 25°C in the presence of 50 μM $CuCl_2$. In experiments where the effect of oxidation was measured after dilution of the reduced protein from denaturant (Figures 4C and 4D), DTT was first removed from the denatured protein by passing through Micro-Biospin 6 column, equilibrated with degassed and nitrogen saturated denaturing buffer (6 M GuHCl). The denatured protein was then diluted 100-fold into degassed and nitrogen saturated buffer A or B, followed by addition of the oxidizing agent (5 μM $CuCl_2$) within 5 s. To analyze the speed of disulfide bond formation, the charge state distribution of reduced and oxidized DM-MBP cysteine mutants was analyzed by LC-MS. For this purpose, 100 μM denatured DM-MBP cysteine mutants (in 6 M GuHCl/10 μM DTT) was diluted 50-fold into buffer B, followed by the addition of $CuCl_2$ after 30 s and inhibition of refolding and disulfide formation 5 s later by addition of 6 M GuHCl pH 2.5 (final GuHCl 4.8 M). Samples were immediately subjected to LC-MS as described below. Quenching of disulfide bond formation was efficient because no oxidized protein was detected when $CuCl_2$ was added after 6 M GuHCl pH 2.5.

Maltose Binding

To analyzed the ability to bind maltose, purified DM-MBP and its cysteine mutants (25 μM) (reduced or oxidized) were either diluted 50-fold into buffer B (native proteins, N) or denatured in 3 M GuHCl and refolded for 90 min upon 50-fold dilution into buffer B (final 500 nM MBP) (refolded proteins, R) (see Figure S4B). The samples were added to 100 μl amylose beads, equilibrated in buffer B, and incubated for 20 min at 25°C with gentle rocking. After a quick spin on a microfuge, the supernatant was removed and the beads washed with 500 μl buffer B. The bound protein was eluted with buffer B containing 50 mM maltose. Eluates were analyzed by 12.5% SDS-PAGE and Coomassie staining.

Rubisco Refolding

Spontaneous and GroEL-assisted refolding of Rubisco at final Rubisco concentrations of 10 nM, 25 nM, 50 nM and 100 nM at 9.5°C and 15°C were performed as described previously (Brinker et al., 2001) with minor modifications. Typically, 1 μM, 2.5 μM, 5 μM, 10 μM Rubisco were denatured in 6 M GuHCl, 20 mM Tris-HCl (pH 7.8), 1 mM EDTA, 50 mM $NaHCO_3$, 200 mM β-ME (or 10 mM DTT), and 10% glycerol for 1 hr at 25°C respectively, and diluted 100-fold into spontaneous refolding buffer 20 mM Tris-HCl, pH 7.8, 250 mM KCl, 5 mM $Mg(OAc)_2$, 1 mg/ml BSA and 200 mM β-ME (or 10 mM DTT) or into assisted refolding buffer (20 mM Tris-HCl, pH 7.5, 20 mM KCl, 5 mM $Mg(OAc)_2$, 1mg/ml BSA and 200 mM β-ME (or 10 mM DTT)). Note that the presence of BSA was without effect on the rate of folding but improved the yield, presumably by preventing the absorption of Rubisco to tube walls (Figure S3E). For the spontaneous reaction, 50-fold molar excess of Rubisco mutant K168E was added to accelerate assembly. At the times indicated, aliquots (40 μl) were withdrawn and rapidly mixed with 10-fold molar excess of GroEL mutant D87K to trap the denatured Rubisco. Assisted refolding was carried out in the presence of 2- or 10-fold molar excess of GroEL and initiated by adding 2-fold molar excess of GroES over GroEL and 5 mM ATP. Aliquots (40 μl) were rapidly mixed with solution containing 7.5 mM CDTA and apyrase (10 U) to stop GroEL action and Rubisco folding.

Rubisco enzyme activity was determined after incubation at 25°C for 1.5 hr (for 10 nM and 25 nM Rubisco) or 1 hr (for 50 nM and 100 nM Rubisco) as described by Goloubinoff et al. (1989) with modifications. 50 mM $Mg(OAc)_2$ was added to the enzyme assay to compensate for the presence of CDTA. To determine the yield of refolding in these experiments, native Rubisco was treated by the same procedure, except that GuHCl was omitted.

Unfolding Kinetics by Stopped-Flow Measurements

The rate of unfolding of WT-MBP, DM-MBP and reduced (red.) and oxidized (ox.) DM-MBP cysteine mutants at various concentrations of GuHCl in buffer A was monitored in stopped-flow mixing experiments using an Applied Photophysics SX.18MV instrument with a 1:1 mixing ratio at 25°C. The dead time of the instrument was ~3 ms. The decrease in fluorescence at 345 nm with an excitation at 295 nm was followed. The rate obtained is an average of 10–20 independent measurements. The final protein concentration was 500 nM. Unfolding rates in the absence of denaturant were determined by extrapolation.

Single-Molecule Experiments

Fluorescence Correlation and Cross-correlation Spectroscopy

For correlation experiments, a DM-MBP double cysteine mutant (DM-MBP(52-298)) was fluorescently labeled either with Atto532 maleimide or Atto647N maleimide (ATTO-TEC) using standard procedures (Sharma et al., 2008).

Fluorescence correlation spectroscopy (FCS) measurements using pulsed interleaved excitation (PIE) (Muller et al., 2005) were performed either on a confocal system based on an inverted microscope (Nikon TE2000) or on a Microtime 200 instrument (PicoQuant GmbH) to analyze the oligomeric state of DM-MBP during spontaneous refolding. Diffusion times of 10 nM DM-MBP(52-298), labeled with Atto532 at both positions, through the confocal volume (1 femtoliter) with or without 1 or 2 μM unlabeled DM-MBP(52-298) were measured by FCS. Atto532 labeled DM-MBP(52-298) bound to GroEL was used as a control. Measurements were taken at 20°C within the first 800 s after initiating refolding by 100-fold dilution from 3 M GuHCl into buffer A. The FCS curves were fitted using Origin 8.0 (OriginLab, Northampton) with the following model Equation (5):

$$y = \frac{\gamma}{N}\left(1+\frac{\tau}{\tau_D}\right)^{-1}\left(1+\frac{1}{\rho^2}\frac{\tau}{\tau_D}\right)^{-1/2} \times \left(1+Ae^{-(\tau/\tau_A)^{\beta}}\right)+y_o \quad (5)$$

for freely diffusing particles with a characteristic diffusion time τ_D through the confocal volume characterized by the structure parameter $\rho = \frac{w_0}{z_0}$ where w_0 and z_0 are related to the radial and axial dimensions of the confocal spot. N describes the average number of particles in the confocal volume $(V_{eff} = (\frac{\pi}{2})^{\frac{3}{2}} w_0^2 z_0)$ and the factor γ corrects for geometrical effects (in the case of a three dimensional Gaussian, $\gamma = 2^{-3/2}$). The stretched exponential with widthβ compensates for afterpulsing of the detectors. Timescales of afterpulsing τ_A were typically on the order of 1 μs. y_o corrects for a non-zero baseline due to slow variations during the experiment and was typically on the order of $\pm\ 10^{-3}$. The diffusion (D) given by Equation (6),

$$D = \frac{w_o^2}{4\tau_D} \quad (6)$$

Fluorescence cross-correlation spectroscopy (FCCS) measurements were performed under refolding conditions as above with a 1:1 mixture of Atto532 labeled DM-MBP(52-298) and Atto647N labeled DM-MBP(52-298) (labeled at position 52) at final concentration of ~5 nM each. For the Microtime, two pulsed lasers (LDH-P-FA-530 (green), LDH-P-C-640B (red), PicoQuant GmbH) were alternated for excitation. The excitation light was focused on the sample by UPlanSApo 60x/1.20 (OLYMPUS) water immersion objective. The laser power at the objective was 30 μW for the FCS and FCCS experiments. The fluorescence emission was focused on the confocal pinhole (diameter 50 μm) and subsequently split by a dichroic mirror (600 dcxr, Semrock). Scattered laser light was blocked by using emission filters. The fluorescent light was detected by two avalanche photodiodes (Micro Photon Devices srl) coupled to a time-correlated single-photon counting device (HydraHarp 400, PicoQuant GmbH) operated in time-tagged time resolved mode (TTTR), which was synchronized to the same 40 MHz master clock used for driving the alternated laser pulses. The cross-correlation functions were calculated by correlating the photons produced by the green excitation laser and detected in the green channel with the photons produced by the red excitation laser and detected in the red channel. In this way, spectral crosstalk can be removed, making FCCS much more sensitive to weak interactions. A double-labeled DNA oligomer (40 base-pair), labeled with Atto532 in one strand and Atto647 in the other at a 22 base-pair separation (IBA GmbH, Germany), was used as a positive control for cross-correlation and the free dyes were measured as a negative control.

Single-Pair FRET

Single-pair FRET (SpFRET) measurements were performed on either the home-built system or the Microtime 200 using PIE (Muller et al., 2005; Sharma et al., 2008). DM-MBP double cysteine mutant (DM-MBP(52-298)) was labeled with Atto532 maleimide (position 52) and Atto647N maleimide (position 298) as previously described (Sharma et al., 2008). The concentration of double-labeled protein in the sample was diluted to ~100 pM to ensure that the probability of having more than one particle in the probe volume at the same time is small. Hence, for each particle detected, the probability of a second particle being in the volume simultaneously is < 1%. For each experiment, at least 500 particles were measured and the experiments were repeated with different protein preparations to verify the reproducibility of the results. Further details regarding the SpFRET measurements and sample preparation are provided in Sharma et al. (2008) and in Supplemental Experimental Procedures therein.

Static and Dynamic Light Scattering

Protein samples (1 μM) were analyzed using static and dynamic light scattering by auto-injection of the sample into the apparatus at a flow rate of 0.2 ml/min (system buffer: 20 mM Tris-HCl pH 7.5, 200 mM KCl, 5 mM $Mg(OAc)_2$, 10 mM maltose, 50 mM GuHCl) at

25°C online with DAWN EOS multi-angle light scattering (Wyatt Technology, 690 nm laser) and variable wavelength UV absorbance (set at 280 nm; Agilent 1100 series) detectors (Wyatt, 1993). The protein sample (900 μl) reaches the detectors 5 min after injection by the autosampler (Agilent 1100 series). DM-MBP (60 μM) denatured in 3 M GuHCl was diluted 60-fold into buffer (20 mM Tris, pH 7.5, 200 mM KCl, 5 mM $Mg(OAc)_2$, 10 mM maltose) and injected 1 to 60 min after initiating refolding. Accordingly light scattering begins to be recorded at 6 to 65 min after initiating refolding. UV absorbance showed that the protein concentration was similar for each measurement at the peak of the scattering signal. Native DM-MPB and Rubisco were mixed at various molar ratios with regard to protomer and adjusted to a final total protein concentration of 1 μM. Protein mass and the hydrodynamic radii were calculated using the ASTRA software (Wyatt Technology) with the dn/dc value for protein set to 0.185 ml/g. Bovine serum albumin was used as the calibration standard.

Mass Spectrometric Analysis

H/D Exchange

Frozen MBP samples (75 μl) from H/D exchange pulse labeling were thawed rapidly within 1 min and immediately injected into a custom built cooled microflow HPLC system (designed by John. R. Engen, Barnett Institute, Boston) at a flow rate of 60 μl/min. Proteins were desalted for 2 min on a 1 mm × 50 mm Vydac C-4 column and directly eluted into the mass spectrometer with an 8 min gradient of 40%−75% acetonitrile. The mobile phase contained 0.1% formic acid. The C-4 analytical column, as well as the injection and switching valves were maintained at ~0°C by placing them in a cooled housing. The mobile phases were precooled through stainless steel loops within a thermoelectric cooling device. Mass spectral analyses were carried out on a Waters Synapt HDMS ESI-QToF mass spectrometer. Capillary voltage was set to 3.2 kV. The ESI source and desolvation temperatures were 50°C and 175°C, respectively, with a desolvation gas flow of 600 l/hr and a cone gas flow of 50 l/hr. Mass spectra were acquired using a 1 s scan time. All QToF data were collected in ESI (+) and V mode. Protein mass spectra were corrected online using a solution of myoglobin (4 pmol/μl) as lock mass. Masses were calculated by deconvoluting multiple charge states of combined protein spectra using MassLynx software and the MaxEnt1 algorithm (Wales and Engen, 2006).

Charge-State Distribution

MBP samples (75 μl) were injected onto a 1 mm x 50 mm Vydac C-4 column and analyzed as above.

SUPPLEMENTAL REFERENCES

Goloubinoff, P., Christeller, J.T., Gatenby, A.A., and Lorimer, G.H. (1989). Reconstitution of active dimeric ribulose bisphosphate carboxylase from an unfolded state depends on two chaperonin proteins and MgATP. Nature *342*, 884–889.

Sreerama, N., and Woody, R.W. (2004). Computation and analysis of protein circular dichroism spectra. Methods Enzymol. *383*, 318–351.

Wales, T.E., and Engen, J.R. (2006). Hydrogen exchange mass spectrometry for the analysis of protein dynamics. Mass Spectrom. Rev. *25*, 158–170.

Wyatt, P.J. (1993). Light scattering and the absolute characterization of macromolecules. Anal. Chim. Acta *272*, 1–40.

Zhang, Y.H., Yan, X., Maier, C.S., Schimerlik, M.I., and Deinzer, M.L. (2001). Structural comparison of recombinant human macrophage colony stimulating factor beta and a partially reduced derivative using hydrogen deuterium exchange and electrospray ionization mass spectrometry. Protein Sci. *10*, 2336–2345.

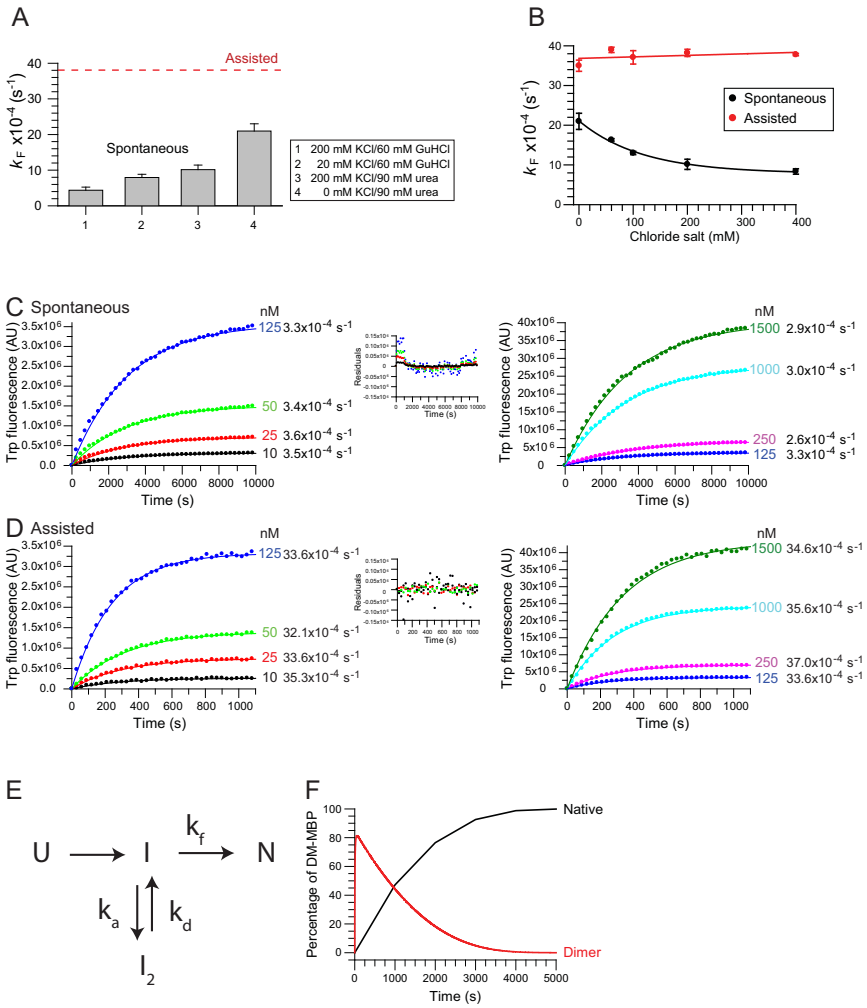

Figure S1. Accelerated Folding by Chaperonin Independent of Aggregation Prevention, Related to Figure 1

(A and B) Effect of chloride salt on spontaneous and assisted refolding of DM-MBP. (A) Rates of spontaneous refolding of DM-MBP at 25°C under varying conditions of chloride salt in the presence of residual concentrations of GuHCl or urea, as indicated. The rate of chaperonin-assisted folding, which is independent of chloride salt or the specific denaturant, is shown as a reference. Standard deviation from at least three independent experiments. (B) Rates of spontaneous and assisted refolding of DM-MBP at varying concentrations of chloride salt in the presence of urea. DM-MBP (25 μM) was denatured in 9 M urea and diluted 100-fold into buffer (100 mM HEPES pH 7.2, 20 mM KOAc, 5 mM $Mg(OAc)_2$) containing the chloride salt (KCl) concentrations indicated either alone (spontaneous) or with 1 μM GroEL/2 μM GroES (assisted) at 25°C. Assisted refolding was initiated by the addition of 2 mM ATP. Refolding was monitored by Trp fluorescence. Standard deviation from 3 independent experiments. Note that aggregation was excluded as the cause of slower refolding at higher salt concentration (see Figures 1D and 1E). Hence, the salt dependence of the spontaneous refolding rate is an intrinsic property of DM-MBP that is unrelated to aggregation. This is consistent with the observation of salt dependent folding in the presence of EL-KKK2/ES chaperonin, which would prevent any aggregation by substrate encapsulation but cannot accelerate DM-MBP folding (see Figure S6C).

(C and D) Rates of spontaneous and assisted folding of DM-MBP. Representative raw data of rates of spontaneous (C) and GroEL/ES-assisted (D) folding of DM-MBP at final concentrations of 10 nM to 1500 nM. DM-MBP was denatured in 6 M GuHCl and diluted 100-fold into buffer A alone (spontaneous) (C) or buffer A containing 2- to 4-fold molar excess of GroEL and 2-fold molar excess of GroES over GroEL (assisted) (D) at 25°C (final 60 mM GuHCl and 200 mM KCl) . Assisted refolding was initiated by the addition of 5 mM ATP. Refolding was monitored by Trp fluorescence at 345 nm. The fluorescence intensity at time 0 was subtracted (see Figures S4C and S4D for unsubtracted data). The apparent rates of folding fitted to a single exponential with R^2 values ranging from 0.993 to 0.999 for spontaneous refolding and 0.973 to 0.999 for assisted refolding. Residuals of the fits are shown for the reactions containing 10 to 125 nM DM-MBP. Rates are indicated next to the respective folding curves. The amplitudes of the final fluorescence increased linearly with the concentration of DM-MBP. Yields were 80%–100% as compared to native DM-MBP controls and based on maltose binding assays (see also Figures S4B–S4D).

(E) Simulation of spontaneous refolding limited by reversible aggregation. A simple model of reversible aggregation involving the formation of a dimeric species (I_2) was used to simulate folding kinetics limited by the reversible formation of non-native oligomers. The rate of formation and dissociation of the dimeric species is given by k_a and k_d, respectively. The folding rate k_f, unimpaired by aggregation, is given by the refolding rate of protein inside the GroEL/GroES cavity, ~0.004 s^{-1} ($t_{1/2}$ ~170 s), as measured for DM-MBP(52-298) labeled with Atto532 at position 52 (Sharma et al., 2008).

(F) Numerical kinetic simulations of refolding using the model in (E) were performed while keeping the concentration of DM-MBP fixed at 10 nM. Varying the rate of formation (k_a) and dissociation (k_d) of the dimeric aggregate species (I_2) showed that the apparent refolding rate was dependent only on the equilibrium

dissociation constant (K_D) of the dimer rather than on the individual values of k_a and k_d. At a K_D of 0.4 nM, the rate of folding matched the experimentally observed rate of spontaneous refolding of DM-MBP(52-298) labeled with Atto532 at position 52 (Sharma et al., 2008) of ~0.0007 s^{-1} ($t_{1/2}$ ~1000 s).

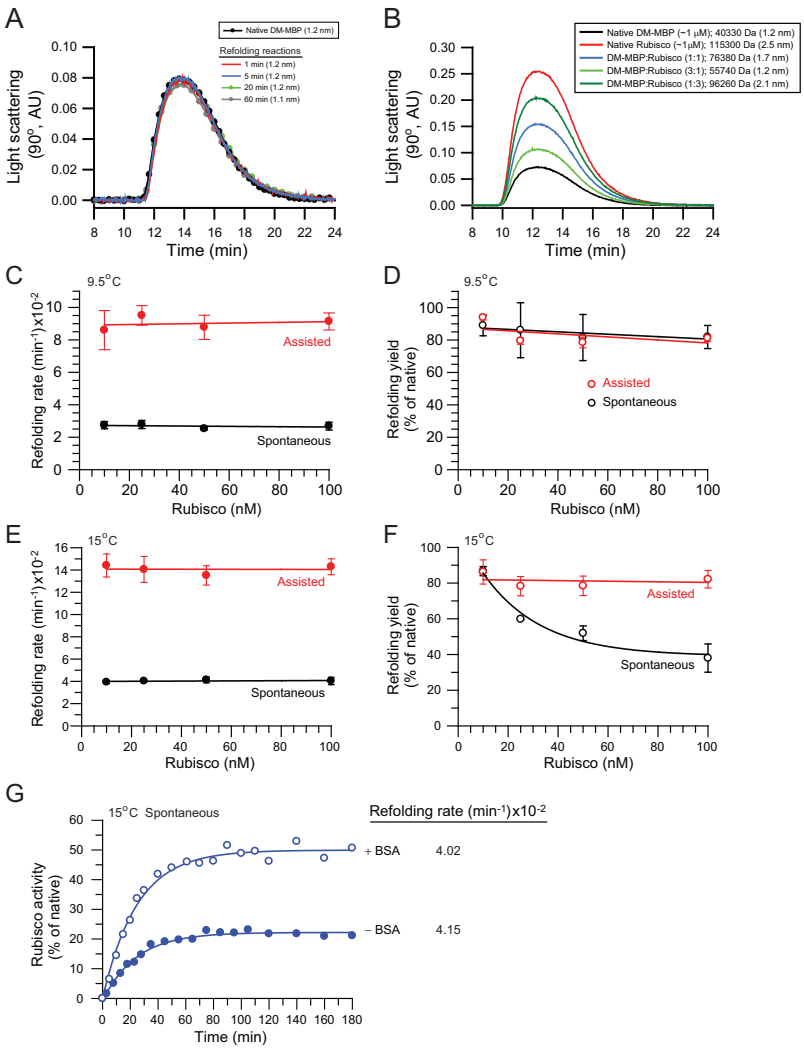

Figure S2. Accelerated Folding by Chaperonin Independent of Aggregation Prevention, Related to Figure 1

(A and B) Light scattering analysis of DM-MBP. Absence of aggregates during spontaneous DM-MBP refolding was also demonstrated by static and dynamic light scattering measurements. (A) Light scattering measurements collected at an angle of 90° for native DM-MBP (~1 μM) and of DM-MBP spontaneously refolding at various times after the initiation of the refolding reaction are shown. Denatured DM-MBP in 3 M GuHCl was diluted 60-fold to a final concentration of ~1 μM. Numbers in parenthesis refer to the hydrodynamic radii measured for the respective samples. The light scattering signal, the hydrodynamic radius and molar mass of the refolding DM-MBP remained equivalent to that of the native protein. (B) Light scattering measurements collected at an angle of 90° are shown. Molar mass and the hydrodynamic radius of native DM-MBP, dimeric Rubisco and various molar ratios of the two proteins (protomer concentrations) is indicated. Final total concentrations are adjusted to ~1 μM (see Extended Experimental Procedures for details). Using dimeric bacterial Rubisco (~55 kDa monomer) as a control protein, the presence of ~15% DM-MBP dimers (~80 kDa) as the smallest possible aggregate would have resulted in a detectable increase in light scattering. These results are in contrast to a recent study reporting the detection of aggregates by light scattering upon DM-MBP refolding at 100 nM (Apetri and Horwich, 2008). However, the scattering signal reported did not decay within the time-scale of refolding and thus is inconsistent with the proposed presence of reversible DM-MBP aggregates as the cause of slow spontaneous folding.

(C–G) Spontaneous and assisted refolding of Rubisco. Rates and yields of spontaneous and GroEL/GroES-mediated refolding of bacterial Rubisco at final concentrations of 10 nM to 100 nM (C–F). Rubisco was denatured in 6 M GuHCl and diluted 100-fold into buffer alone (spontaneous) or buffer containing 2 to10-fold molar excess of GroEL and 2-fold molar excess of GroES over GroEL (assisted) at ~9.5°C (C and D) or ~15°C (E and F). Assisted refolding was initiated by the addition of 5 mM ATP. Refolding was assayed by recording enzymatic activity. Yields are expressed as percent of native control. Standard deviation from three independent measurements (see Extended Experimental Procedures for details).

(G) Spontaneous refolding of 100 nM Rubisco in the absence or presence of BSA (~15 μM) at 15°C. Activities are expressed as a percentage of the activity of 100 nM native Rubisco. Since denatured Rubisco tends to aggregate and adsorb to tube walls, BSA is routinely present in refolding reactions to limit non-specific protein loss. It was recently suggested that BSA modulates Rubisco aggregation, perhaps favoring the formation of reversible aggregates during spontaneous refolding (Apetri and Horwich, 2008). Upon repeating the refolding reactions with and without BSA, we observed that the apparent rate of spontaneous refolding remained unchanged, but the folding yield was significantly reduced in the absence of BSA, supporting our conclusion that aggregate formation and/or adsorption to tube walls is irreversible at the timescale of folding.

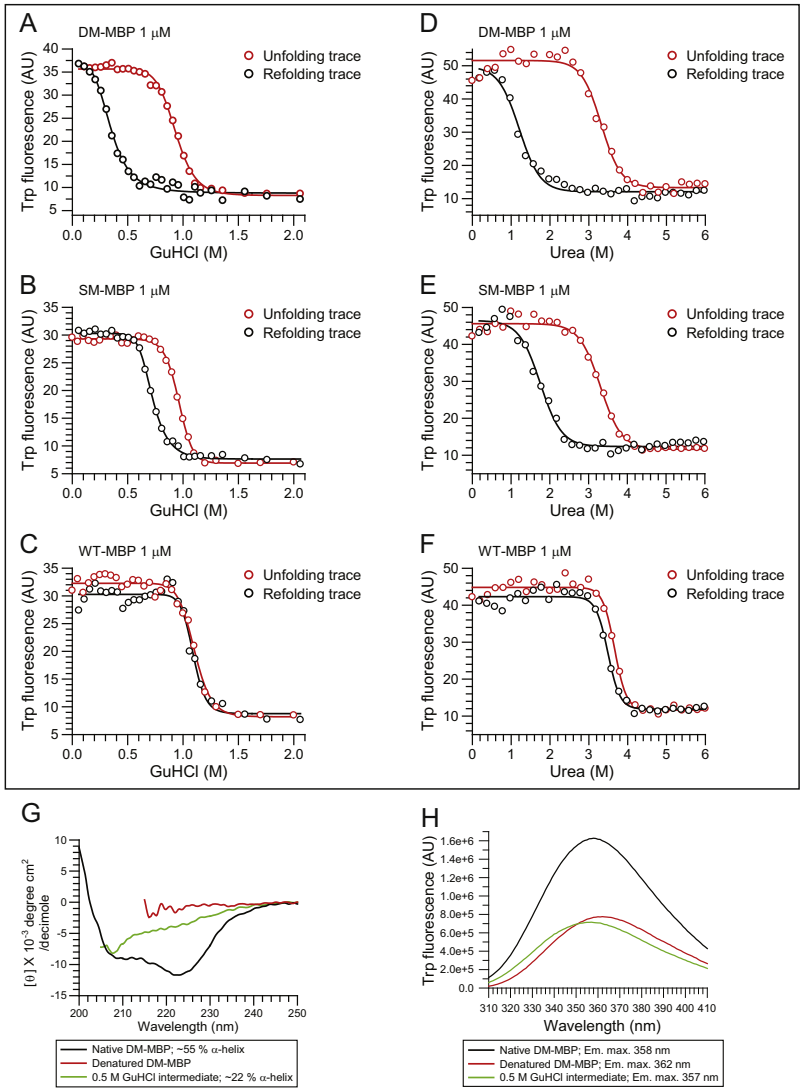

Figure S3. Characterization of a Kinetically Trapped Refolding Intermediate of DM-MBP, Related to Figure 2

(A–F) GuHCl-dependent unfolding and refolding of MBP. Unfolding and refolding of DM-MBP, SM-MBP and WT-MBP (1 μM each) was monitored by Trp fluorescence with excitation at 295 nm and emission at 345 nm. Unfolding trace: native MBP was incubated for 12 hr with increasing concentrations of GuHCl in buffer A at 25°C. Refolding trace: MBP (100 μM) was unfolded in 6 M GuHCl and then diluted 100-fold into buffer A containing increasing concentrations of GuHCl, followed by incubation for 12 hr at 25°C. Representative measurements from at least two independent experiments.

(G) Circular dichroism wavelength scans. CD wavelength scans of native, denatured and 0.5 M GuHCl intermediate of DM-MBP (2 μM) measured at 25°C with 0.1 cm cuvettes.

(H) Trp fluorescence wavelength scans. Trp fluorescence of native, denatured and 0.5 M GuHCl intermediate of DM-MBP (250 nM each) at 25°C. Emission maxima are indicated.

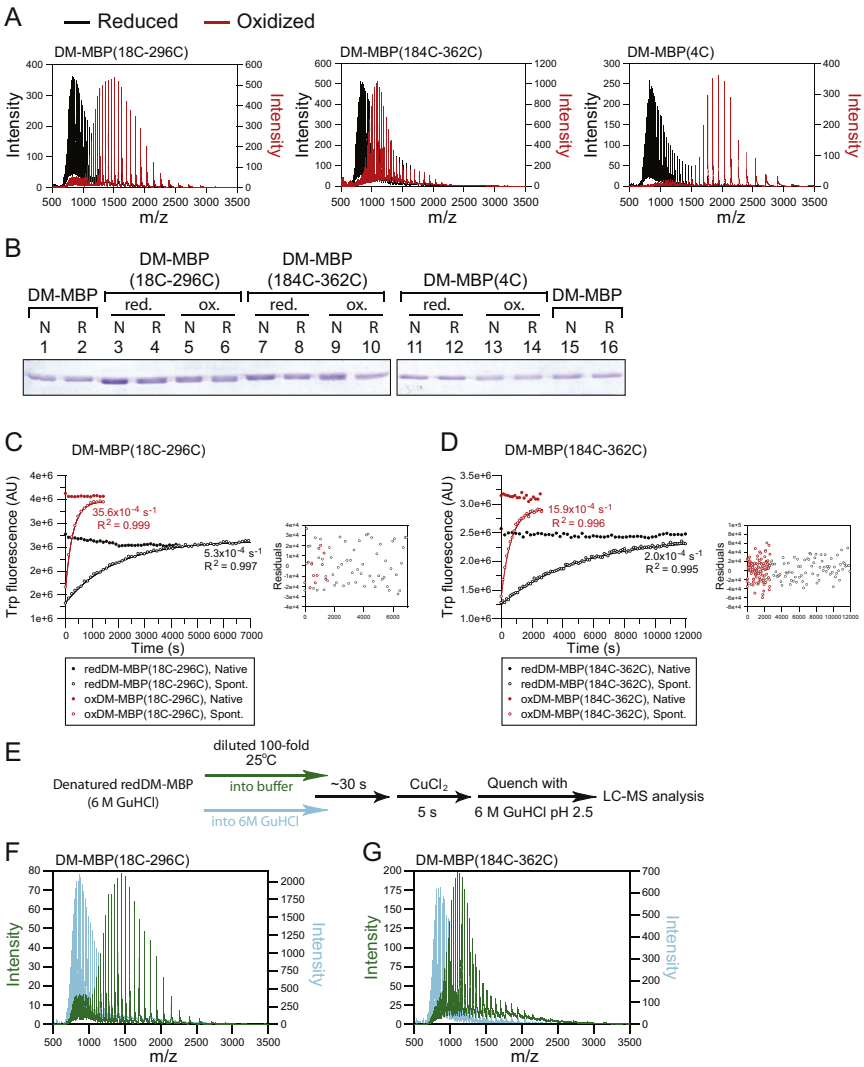

Figure S4. Characterization of Cysteine Pair Mutants of DM-MBP, Related to Figure 4 and Figure 5

(A) Charge state distribution measured by LC-MS. DM-MBP(18C-296C), DM-MBP(184C-362C), and DM-MBP(4C) were analyzed under reducing and oxidizing conditions on a Waters Synapt HDMS ESI-QToF mass spectrometer. The distribution of the charge state centers distinguishes between the reduced (black) and disulfide-bonded proteins (red) (Zhang et al., 2001).

(B) Affinity of maltose binding. Native (N) and spontaneously refolded (R) DM-MBP, as well as reduced (red.) and oxidized (ox.) DM-MBP(18C-296C), DM-MBP(184C-362C) and DM-MBP(4C) (final 500 nM) were incubated with amylose beads for 20 min at 25°C. Bound protein was eluted by addition of buffer B/50 mM maltose and samples were analyzed by 12% SDS-PAGE and Coomassie staining.

(C and D) Single exponential rates of refolding of DM-MBP cysteine mutants. Representative raw data of rates and yields of spontaneous refolding of DM-MBP(18C-296C) (C) and DM-MBP(184C-362C) (D) at final concentration of 250 nM. Reduced (red.) or oxidized (ox.) DM-MBP cysteine mutants were denatured in 6 M GuHCl and diluted 100-fold into buffer A at 25°C. Refolding was monitored by Trp fluorescence at 345 nM. Note that the Trp fluorescence of the reduced proteins (black curves) is quenched relative to the oxidized proteins (red curves).

The apparent rates of folding fitted to a single exponential. The residuals of the fits are shown in the inserts. Rates and R^2 values of the fits are indicated next to the respective folding curves. The fluorescence intensities of native protein controls are shown. Refolding yields were between 80%–100%.

(E–G) Rapid disulfide-bond formation upon protein collapse. Schematic representation of the experiment (E). Reduced (red.) DM-MBP(18C-296C) (F) and DM-MBP(184C-362C) (G) (final ~2 μM) were unfolded in 6 M GuHCl and diluted 50-fold into either buffer B (green) or buffer B containing 6 M GuHCl (blue), followed by the addition of $CuCl_2$ after 30 s. Refolding was stopped 5 s later by addition of 6 M GuHCl, pH 2.5, followed by LC-MS analysis as described in Extended Experimental Procedures.

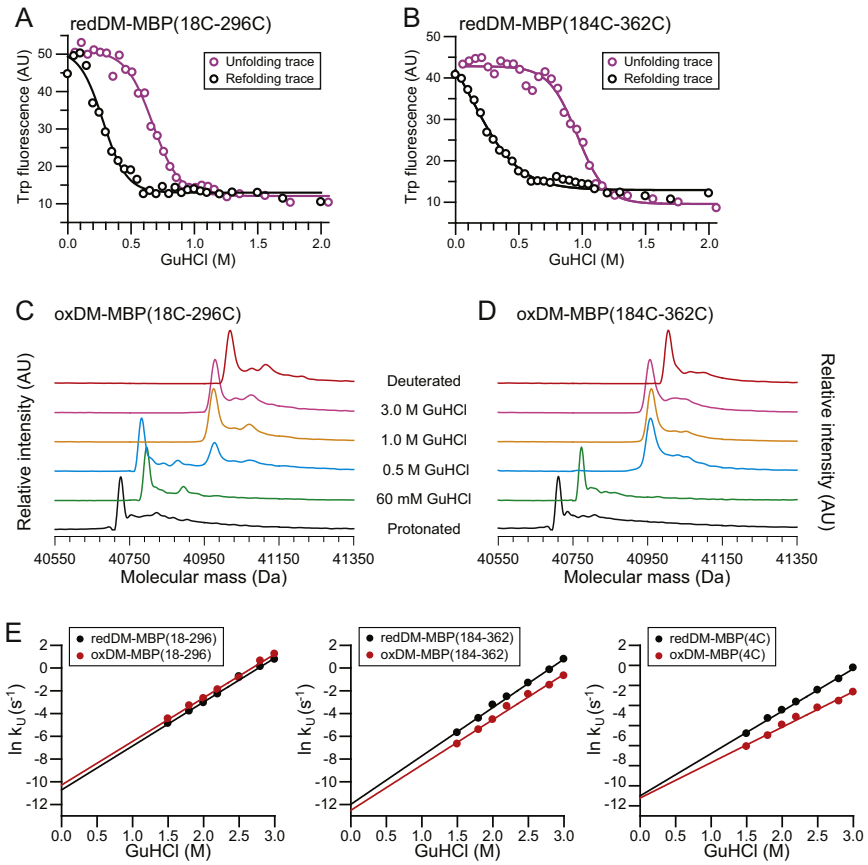

Figure S5. Characterization of Cysteine Pair mutants of DM-MBP, Related to Figure 4 and Figure 5

(A and B) GuHCl-dependent unfolding and refolding. Unfolding and refolding of reduced (red.) DM-MBP(18C-298C) (A) and redDM-MBP(184C-362C) (B) was monitored by Trp fluorescence after incubation at different GuHCl concentrations for 12 hr at 25°C (see Figures 4E and 4F).

(C and D) Characterization of the kinetically trapped refolding intermediate of DM-MBP cysteine mutants by H/D exchange. Pulsed H/D exchange after incubation in different denaturant concentrations. Deconvoluted mass spectra of oxidized (ox.) DM-MBP(18C-296C) (C) and oxDM-MBP(184C-362C) (D) as a function of denaturant monitored by ESI-QToF mass spectrometry. Proteins were diluted from 3 M GuHCl into buffer B to the final GuHCl concentrations indicated. After incubation for 12 hr samples were subjected to a 10 s deuterium pulse. The native protonated and deuterated proteins are shown as reference (see Experimental Procedures for details).

(E) Kinetics of unfolding. The rate of unfolding of WT-MBP, DM-MBP and reduced (red.) and oxidized (ox.) DM-MBP cysteine mutants at different concentrations of GuHCl in buffer A was monitored in stopped-flow mixing experiments at 25°C by following the decrease in Trp fluorescence at 345 nm. The final protein concentration was 500 nM. Unfolding rates in the absence of denaturant were determined by extrapolation.

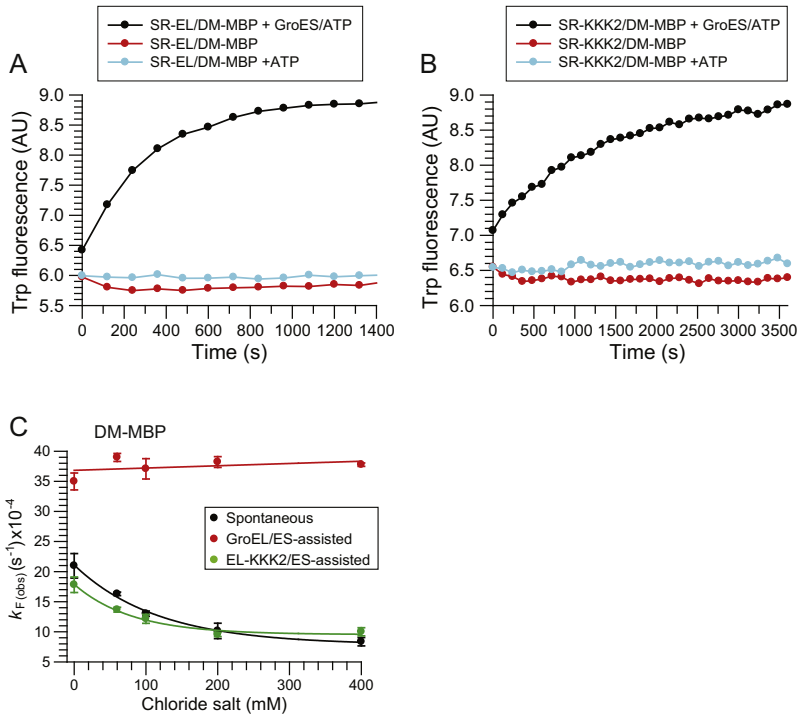

Figure S6. Characterization of SR-KKK2 Mutant, Related to Figure 6

(A and B) Binding affinity of the SR-KKK2 mutant for DM-MBP. Refolding of GuHCl-denatured DM-MBP (25 μM) at 25°C upon 100-fold dilution into buffer B containing 1.0 μM SR-EL or SR-KKK2 (red); 1.0 μM SR-EL/2 mM ATP or SR-KKK2/2 mM ATP (blue); 1.0 μM SR-EL/2 μM GroES/2 mM ATP or SR-KKK2/2 μM GroES/2 mM ATP (black). Inhibition of spontaneous DM-MBP refolding by SR-KKK2 (and SR-EL) in the presence of ATP but absence of GroES indicates that SR-KKK2 has a similar affinity for DM-MBP as SR-EL (or GroEL) (Tang et al., 2006, 2008).

(C) Effect of chloride salt on spontaneous and assisted refolding of DM-MBP. Rates of spontaneous and assisted refolding of DM-MBP at varying concentrations of chloride salt. DM-MBP (25 μM) was denatured in 9 M urea and diluted 100-fold into buffer (100 mM HEPES pH 7.2, 20 mM KOAc, 5 mM $Mg(OAc)_2$) containing the chloride salt (KCl) concentrations indicated either in the absence of GroEL (spontaneous), with 1 μM GroEL/2 μM GroES or with 1 μM EL-KKK2/2 μM GroES at 25°C (assisted). Assisted refolding was initiated by the addition of 2 mM ATP. Refolding was monitored by Trp fluorescence. Standard deviation from three independent experiments.